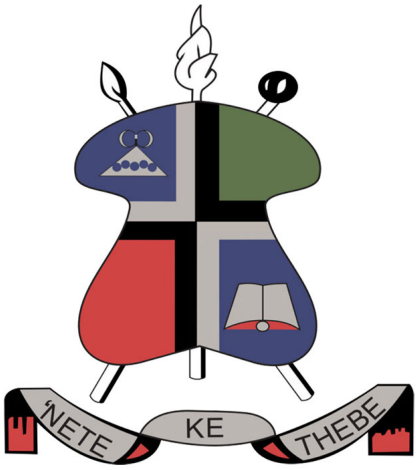

NATIONAL UNIVERSITY
OF LESOTHO

Mathematical model of oncolytic virus resistance with allee effect

by

Thethe Likhang (202000312)

Dissertation presented in fulfilment of the academic requirements
at the National University of Lesotho
for the degree of

Bachelor of Science-Honors in Applied Mathematics

Department of Mathematics and Computer Science
National University of Lesotho

Supervisor: Dr. Khaphetsi Joseph Mahasa,
Department of Mathematics and Computer Science,
National University of Lesotho, Roma, Maseru, Lesotho.

22 June 2026

Declaration

I, Likhang Thethe, hereby declare that this dissertation has not been submitted in whole or in part for any academic qualification. This dissertation is my own personal work. All significant contributions to, and all quotations from other sources within this dissertation, have been adequately acknowledged and properly cited.



----  ----

Date: 22nd June 2026.

Copyright ©2026 National University of Lesotho
All rights reserved

Abstract

Oncolytic virotherapy (OVT) is a promising cancer treatment, yet its long-term efficacy is heavily undermined by the emergence of therapy-resistant tumor cell populations. This study introduces a mathematical model to investigate the coupled dynamics of oncolytic virus infection, tumor resistance, and the Allee effect. The findings show that while high viral infection rates efficiently deplete susceptible tumor cells, they concurrently trigger competitive release, driving the rapid proliferation and dominance of resistant clones. Crucially, the integration of the Allee effect exploits the ecological vulnerabilities of the tumor to counter this resistance. A strong Allee effect establishes a definitive critical density threshold that guarantees absolute multi-clonal tumor extinction once virotherapy drives the population to microscopic levels. Simultaneously, a substantial weak Allee effect severely penalizes the growth rate of emerging resistant strains, keeping them clinically stagnant even when spatial and nutritional resources become available. These results suggest that maximizing viral infectivity alone is insufficient for complete tumor eradication; instead, successful OVT protocols must be strategically designed to drive interacting tumor subpopulations below their critical Allee thresholds to achieve permanent clearance.

Dedication

This dissertation has been written with great affection for my dear family, without whose support, understanding, sacrifice, and boundless love, I could not have achieved what I have accomplished so far in academics. My friends and guides deserve mention as well, for their belief and support. None of this would have been possible without you all.

Acknowledgments

Above all, I would like to thank my supervisor for all his advice, immense support, and profound knowledge that helped me carry out this piece of research successfully. The invaluable input he provided has greatly affected my research process and helped me learn more about the mathematical modeling of cancer growth.

Secondly, I wish to say many thanks to the faculty members and administrative staff of my department for the stimulating environment they created and all the resources that helped me conduct this research project.

Thirdly, I want to say thanks to my colleagues and fellow students for fruitful cooperation, helpful criticism, and friendly discussions that have been of great help during this work.

Last but not least, I want to thank the administration of my university for the effective assistance and valuable support during my research process.

Contents

Declaration . . . . . **ii**

Abstract . . . . . **iii**

Dedication . . . . . **iv**

Acknowledgments . . . . . **v**

Contents . . . . . **vi**

List of figures . . . . . **viii**

List of tables . . . . . **ix**

1 Introduction **1**

1.1 Overview of Oncolytic Virotherapy and Tumor Dynamics 1

1.2 Therapy Resistance and Competitive Release in Virotherapy 2

1.3 Motivation of the Study 3

1.4 Overall Aim of the Study 3

1.5 Objectives of the Study 3

1.6 Methodology 4

1.7 Outline of the study 4

2 Background Literature **6**

2.1 Historical Foundations of Oncolytic Virotherapy Modeling 6

2.2 Tumor Heterogeneity and Mechanisms of Viral Resistance 7

2.3 The Allee Effect in Cancer Biology 7

2.4 Synthesis and the Identified Research Gap 8

3 Mathematical model of oncolytic virus resistance with Allee effect . . 9
3.1 Project overview . . . 9
3.2 Key Modeling Aspects . . . 9
3.3 Model Formulations . . . 11
3.4 Boundedness of the Model . . . 14
3.5 Model analysis . . . 17
3.5.1 Derivation of the steady states for the model without Allee effect . 17
3.5.2 Calculation of the Basic Reproduction Number ($\mathcal{R}_0$) . . . 18
3.5.3 Next-Generation Matrix . . . 19
3.5.4 Stability Analysis of the Extinction State $\mathcal{S}_0$ . . . 20
3.5.5 Stability Analysis of the Uninfected Tumor State $\mathcal{S}_1$ . . . 21
3.5.6 Stability Analysis of $\mathcal{S}_2 = (0, K, 0, 0)$ . . . 23
3.5.7 The Coexistence State $\mathcal{S}_3$ . . . 23
3.5.8 The Viral Threshold State $\mathcal{S}_4$ . . . 24
3.5.9 The Endemic Equilibrium State $\mathcal{S}_5$ . . . 26
3.6 Simulations . . . 29
3.6.1 Model Dynamics without Allee effect . . . 29
3.6.2 Model dynamics with Allee effect . . . 31

4 Conclusions . . . 40
4.0.1 Limitations and future work . . . 41

Bibliography . . . 43

List of Figures

1.1 **Schematic representation of oncolytic virotherapy dynamics.** . . . 2

3.1 **Schematic diagram of the model** 10
3.2 **Model dynamics without Allee effect during OVT.** 29
3.3 **Phase potrait and $Tu-V$ Lag Analysis of the model without Allee effect.** 30
3.4 **Allee effect on uninfected tumor cell population during OVT.** . . 32
3.5 **Allee effect on reistant tumor cell population during OVT.** 34
3.6 **Allee effect on infected tumor cell population during OVT.** 36
3.7 **Allee effect on Free Oncolytic Viruses during OVT.** 38

List of Tables

3.1 **Description of parameters involved in the model** 14
3.2 **Model Parameters: Baseline Values and Ranges Used in Model Simulations** 14

Chapter 1

Introduction

Cancer is still one of the leading causes of death worldwide [1–3]. This creates a strong need for treatment methods that go beyond typical chemotherapy. One promising approach is oncolytic virotherapy (OVT) [3–7]. This method uses natural or genetically modified viruses that specifically infect, replicate within, and kill cancer cells while keeping healthy cells intact [3–6, 8, 9].

1.1 Overview of Oncolytic Virotherapy and Tumor Dynamics

The fundamental mechanism of OVT relies on the selective exploitation the abnormal pathways found in cancer cells [5, 6, 8]. As shown in Figure 1.1, normal cells in the host are safe because of their ability to control viral replication, while cancer cells are vulnerable and can be taken advantage of [4]. The virus hijacks the machinery of these tumor cells to replicate until the host cell runs out of energy and eventually dies. This lytic process sets off a chain reaction: when the cell membrane breaks apart, it releases new infectious viral particles into the surrounding tumor area, which can then go on to infect nearby tumor cells [4, 5, 8].

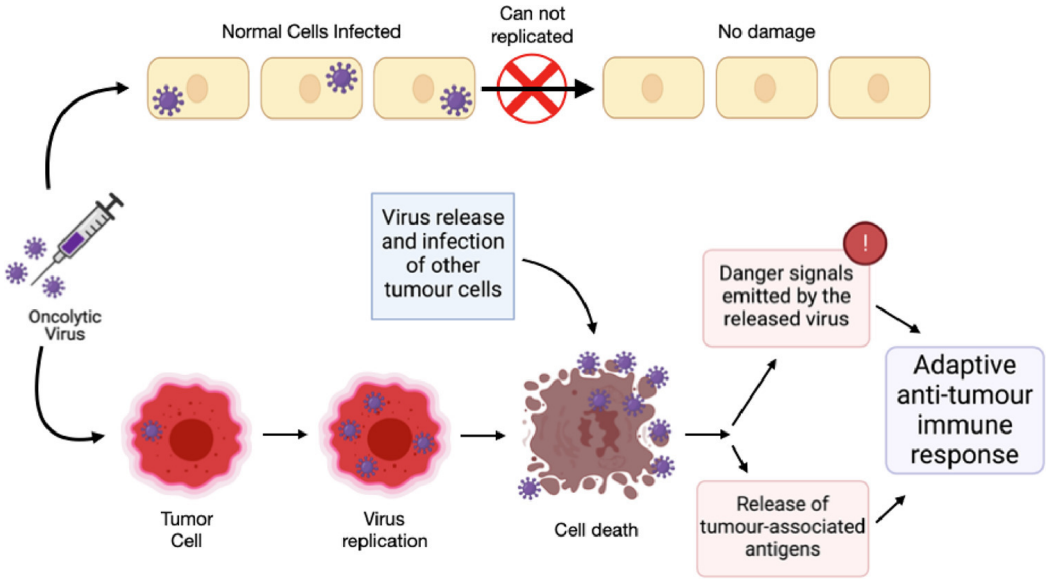

FIG. 1.1. **Schematic representation of oncolytic virotherapy dynamics.**

This illustrates the selectivity of the virus, replication within the tumor, cell destruction, and the ensuing activation of the adaptive immune response against tumors [4].

1.2 Therapy Resistance and Competitive Release in Virotherapy

Despite the solid conceptual design of OVT, its clinical effectiveness is often undermined by the changes that occur with therapeutic resistance. The tumor microenvironment is naturally varied. It consists of different subclonal groups that have different levels of vulnerability to viral infection. When large doses of the virus are given, the treatment quickly wipes out the dominant susceptible subpopulation [2, 10–12].

However, this quick depletion often leads to an ecological event called *competitive release* [2, 11]. By suddenly getting rid of the dominant subpopulation, virotherapy clears out the spatial, structural, and nutritional competition within the tumor environment. This opens up metabolic resources, allowing smaller, virus-resistant clones to grow without restraint, ultimately rebuilding a tumor mass that resists treatment. As a result, focusing only on maximizing viral cytotoxicity can often lead to long-term treatment failures [2, 12].

1.3 Motivation of the Study

This research is motivated by the critical need to design ecologically informed protocols that counter competitive release within heterogeneous tumors. Traditional mathematical models of oncology rely heavily on classical logistic or exponential growth frameworks. While these frameworks capture macro-scale growth accurately, they break down at low cell densities by assuming that a population can always recover exponentially from infinitesimally small numbers [13–15].

In reality, subclonal populations that are significantly depleted encounter challenges related to cooperation and survival when at low densities, a phenomenon known as the Allee effect [16]. A mild Allee effect results in a growth penalty that hinders proliferation at reduced densities, while a pronounced Allee effect establishes a critical density threshold, beneath which the growth rate of the population turns negative, leading to certain localized extinction [13, 15–17]. Traditional models fail to account for these critical thresholds at low densities, consequently exaggerating the resilience of tumors and neglecting an essential ecological weakness [16, 18].

1.4 Overall Aim of the Study

The overall aim of this study is to develop, analyze, and simulate an ecologically grounded mathematical framework that couples the evolutionary dynamics of viral resistance with both weak and strong Allee effects. This framework aims to identify strategies that exploit low-density subclonal thresholds, suppressing competitive release to drive heterogeneous tumor populations into absolute extinction.

1.5 Objectives of the Study

To achieve the primary aim, the study addresses the following specific objectives:

1. To formulate a compartmental system of non-linear ordinary differential equations

(ODEs) modeling the interactions between susceptible tumor cells, resistant tumor cells, and free oncolytic virions under varying Allee effect constraints.

2. To perform qualitative mathematical analysis, including the derivation of equilibria and the evaluation of their local and global asymptotic stability properties.

3. To execute numerical simulations illustrating how the interplay between viral infection rates and Allee thresholds influences subclonal survival.

1.6 Methodology

This study employs deterministic compartmental modeling using a system of nonlinear ordinary differential equations (ODEs) to capture the kinetic interactions within the tumor microenvironment. Qualitative techniques from dynamical systems theory, including stability analysis and bifurcation theory, are applied to determine long-term systemic behavior. Analytical findings are validated through numerical simulations executed using computational softwares, (MATLAB and SageMath), tracking cellular trajectory variations across different Allee thresholds.

1.7 Outline of the study

The remainder of this dissertation is structured to systematically build upon this foundational framework:

Chapter 2: Background Literature. This chapter provides a comprehensive review of the biological principles governing tumor heterogeneity, the mechanisms driving virotherapy resistance, and the ecological theory behind the Allee effect. It also evaluates existing mathematical models that inform the development of this work.

Chapter 3: Mathematical Model of Oncolytic Virus Resistance with Allee Effect. This chapter presents the formulation, qualitative analysis, and numerical simulation of the proposed ordinary differential equation model. The findings demonstrate that in-

tegrating weak and strong Allee effects is critical for predicting complete tumor clearance and preventing the competitive release of resistant sub-populations.

Chapter 4: Conclusions. The dissertation concludes in a comprehensive overview of the fundamental mathematical and oncological insights derived from this study, clearly outlining its contributions to the field of mathematical oncology and proposing significant directions for future developments.

Chapter 2

Background Literature

2.1 Historical Foundations of Oncolytic Virotherapy Modeling

The utilization of mathematical modeling to oncology has a substantial historical background, particularly in quantifying the nonlinear dynamics of oncolytic virotherapy (OVT). Early foundational models established by researchers such as Wodarz [7] and basic frameworks developed later treated viral-tumor interactions using classical predator-prey frameworks [9, 19]. In these deterministic systems of ordinary differential equations (ODEs), uninfected tumor cells act as the prey population, while the replicating virus functions as a self-amplifying predator.

These pioneering models demonstrated that the fundamental efficacy of virotherapy relies heavily on the viral burst size and the infection rate [7]. However, a major theoretical limitation of these early models is their reliance on classical exponential or logistic growth frameworks for the tumor population. Under these assumptions, standard ODE models rarely predict absolute biological eradication; instead, they typically forecast long-term oscillatory behavior or stable coexistence where a residual tumor mass persists indefinitely [20, 21].

2.2 Tumor Heterogeneity and Mechanisms of Viral Resistance

A key barrier to successful clinical outcomes in OVT is tumor heterogeneity [22]. Solid tumors are rarely uniform masses; they are complex ecosystems made up of subclonal cell populations with different levels of genetic and phenotypic diversity. Among these variations, the development of resistance to viral entry, replication, or lysis creates a significant challenge for treatment design [22–24].

Mathematical studies of resistance often emphasize the ecological idea of "competitive release". In an untreated condition, susceptible tumor cells usually dominate the microenvironment because of their better fitness or spatial position. When an aggressive oncolytic virus is introduced, it quickly targets and destroys this susceptible group. However, this targeted destruction unintentionally eases intense spatial and nutritional competition within the tumor niche. The sudden release of resources enables the previously suppressed, resistant subclonal population to grow without restraint, leading to a treatment-resistant relapse [2, 10–12]. Therefore, mathematical models need to expand beyond single-population dynamics to examine the combined evolutionary pressures affecting both susceptible and resistant strains.

2.3 The Allee Effect in Cancer Biology

To understand survival patterns in broken or low-density tumor populations, mathematical oncologists have started to include the Allee effect in growth laws. This concept, introduced by W.C. Allee [25] in population ecology, explains a positive connection between population density and per-capita growth rate at low numbers [26]. In cancer research, this reflects the fact that isolated cancer cells often find it hard to grow without key cooperative mechanisms, such as paracrine growth factor signaling, cellular protective shielding, and tumor-induced angiogenesis [16].

The literature recognizes two types of Allee constraints:

- **Weak Allee Effect:** The per-capita growth rate decreases at low cell densities but stays positive, leading to a temporary halt or delay in tumor growth [13, 27–29].
- **Strong Allee Effect:** This introduces a critical phenotypic density threshold (α_s). If the tumor cell density drops below α_s, the per-capita growth rate turns negative, pushing the subpopulation toward certain extinction [13, 27–29].

Integrating these thresholds helps models explain why small residual disease after treatment doesn't always lead to a larger recurrence. It provides an important tool for evaluating total tumor clearance.

2.4 Synthesis and the Identified Research Gap

Although there are many individual studies on virotherapy resistance frameworks or the mathematical use of allee effects in uniform tumor masses, a significant gap remains where they overlap [13, 20]. Current ordinary differential equation frameworks have not fully explored how a multi-clonal tumor system-which includes different, competitively interacting resistant and susceptible subpopulations-functions when both groups face varying Allee thresholds [15].

This dissertation focuses on this gap. By creating a coupled ODE model that connects oncolytic viral replication, resistance-driven competitive release, and distinct strong and weak Allee thresholds, this work seeks to identify the ecological tipping points that can push both primary and resistant tumor clones toward complete eradication.

Chapter 3

Mathematical model of oncolytic virus resistance with Allee effect

3.1 Project overview

Mathematical models incorporating the Allee effect into oncolytic virotherapy (OVT) describe the complex dynamics of tumor cell and virus populations, revealing how this effect significantly influences the conditions necessary for tumor control or elimination. The Allee effect, where per capita growth rate decreases at low population densities, is a key factor in understanding treatment outcomes and the potential for treatment resistance or failure [13, 17, 30].

3.2 Key Modeling Aspects

1. Model Frameworks: These models typically use systems of nonlinear ordinary differential equations (ODEs) to track populations of uninfected tumor cells (T or U), infected tumor cells (I), and free virions (V). Some models also incorporate immune responses (e.g., T-cells, interferon) [31, 32].

2. Allee Effect Implementation: The Allee effect is integrated into the tumor cell growth

term, often as a function $A(T, \alpha, \omega)$, which modulates the growth rate based on population density [17].

- **Weak Allee Effect**: Growth rate is reduced at low densities but remains positive, so the population can still grow, just more slowly [13, 27–29, 33].
- **Strong Allee Effect**: A critical population threshold (α) exists below which the population growth rate becomes negative, leading to extinction [13, 27–29, 33].

3. Researchers use bifurcation analysis to identify critical thresholds in parameters (e.g., viral infection rate, virus burst size) that lead to different stable states: tumor elimination, tumor persistence/escape, or coexistence (oscillatory dynamics) [34, 35].

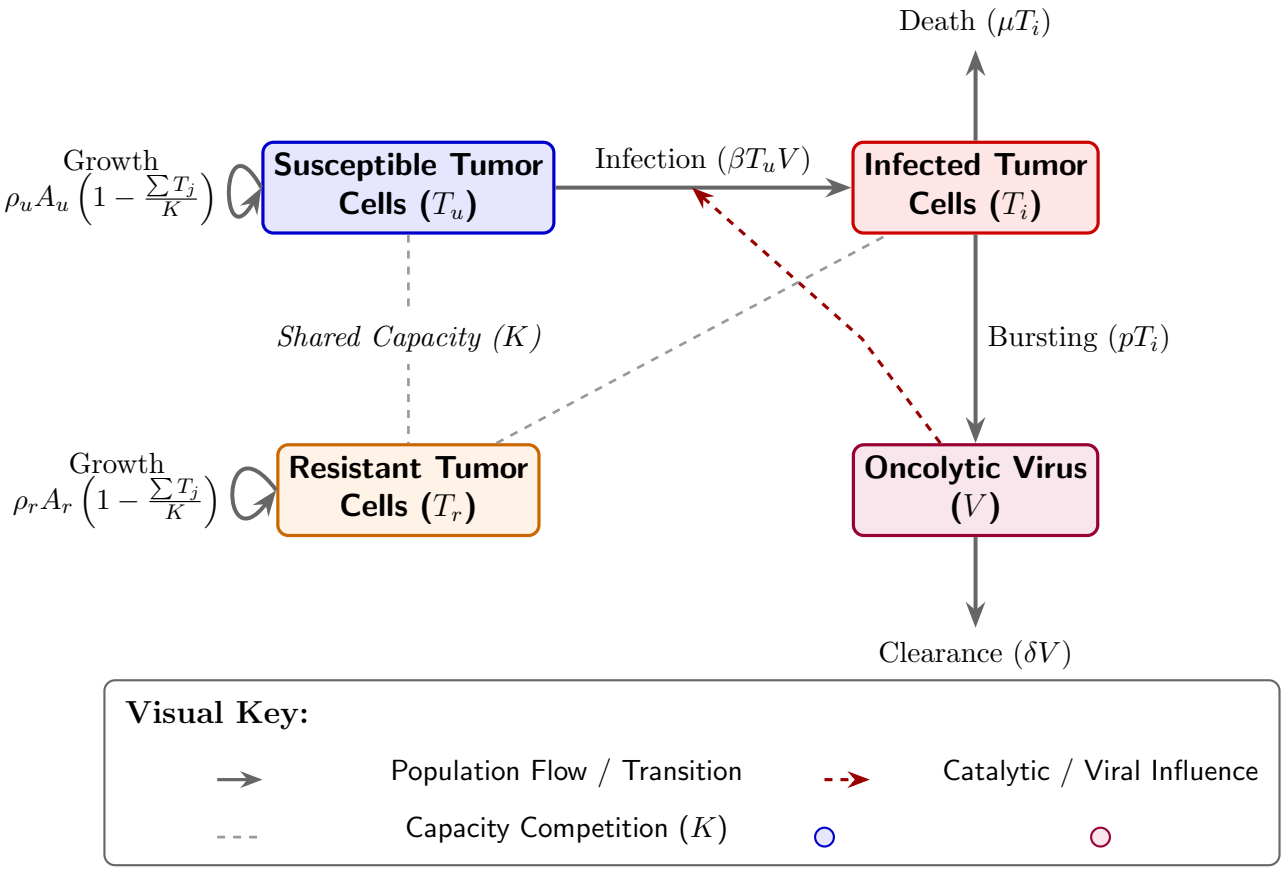

FIG. 3.1. **Schematic diagram of the model**

3.3 Model Formulations

To explore model formulations that include virus-resistant populations, the standard oncolytic virus (OV) model is expanded to incorporate a new variable representing the resistant cells. The Allee effect is then applied to the growth dynamics of both susceptible and resistant tumor cell populations.

The novel model developed in this study involves a system with four variables: Susceptible tumor cells (T_u), resistant tumor cells (T_r), infected tumor cells (T_i), free oncolytic viruses (V).

The system of ordinary differential equations (ODEs) incorporating an Allee effect $A(\dots)$ is given by

$$\frac{dT_u}{dt} = \rho_u T_u \left(1 - \frac{T_u + T_i + T_r}{K}\right)\left(\frac{T_u - \alpha_s}{T_u + \alpha_w}\right) - \beta T_u V, \tag{3.1}$$

$$\frac{dT_r}{dt} = \rho_r T_r \left(1 - \frac{T_u + T_i + T_r}{K}\right)\left(\frac{T_r - \alpha_s}{T_r + \alpha_w}\right), \tag{3.2}$$

$$\frac{dT_i}{dt} = \beta T_u V - \mu T_i, \tag{3.3}$$

$$\frac{dV}{dt} = pT_i - \delta V. \tag{3.4}$$

Here, $A\left(T_j, \alpha_s, \alpha_w\right) = \dfrac{T_j - \alpha_s}{T_j + \alpha_w}$, $j = u, r$ respectively, is a typical Allee effect term for strong and weak effect [13].

A detailed description of the model is as follows;

In Eq. (3.1), the first term

$$\rho_u T_u \left(1 - \frac{T_u + T_i + T_r}{K}\right)\left(\frac{T_u - \alpha_s}{T_u + \alpha_w}\right)$$

describes the intrinsic growth dynamics of susceptible (uninfected) tumor cells in the absence of viral infection [3, 13, 36]. Specifically, tumor cells are assumed to grow logistically with intrinsic proliferation rate ρ_u and carrying capacity K [31], where the total tumor

burden is given by $T_u + T_i + T_r$. The logistic term reflects competition for limited resources within the tumor microenvironment (TME).

The growth is further modulated by the Allee effect term

$$\left(\frac{T_u - \alpha_s}{T_u + \alpha_w}\right),$$

which captures density-dependent limitations at low population sizes. Here, α_s represents the strong Allee threshold, below which the net growth rate becomes negative, leading to extinction of the susceptible tumor population, while α_w controls the smoothness of the transition and allows for weak Allee effects when α_s is small [13, 28, 33]. Biologically, this term accounts for mechanisms such as reduced cell-cell signaling, insufficient vascularization, or impaired cooperative interactions at low tumor densities [16, 17, 33].

The second term, $-\beta T_u V$, represents the infection of susceptible tumor cells by free oncolytic viruses. The infection process is modeled using mass-action kinetics, where β is the infection rate constant. This assumes that the rate of contact between tumor cells and viruses is proportional to their respective populations. Upon infection, susceptible tumor cells transition into the infected class T_i [13, 31, 37].

In Eq. (3.2), the growth of virus-resistant tumor cells T_r is modeled. The first term

$$\rho_r T_r \left(1 - \frac{T_u + T_i + T_r}{K}\right)\left(\frac{T_r - \alpha_s}{T_r + \alpha_w}\right)$$

represents logistic growth with intrinsic rate ρ_r under the same environmental carrying capacity K. Similar to the susceptible population, the resistant cells are also subject to an Allee effect, reflecting that even resistant phenotypes require a minimum population density to sustain growth [16, 17, 38].

Unlike susceptible tumor cells, resistant cells are assumed to be completely refractory to viral infection; hence, no infection or death terms due to virus are included in this equation. This assumption captures the emergence of tumor subpopulations that evade virotherapy due to genetic or phenotypic resistance mechanisms [39, 40].

In Eq. (3.3), the dynamics of infected tumor cells T_i are described. The first term, $\beta T_u V$,

corresponds to the influx of newly infected tumor cells arising from successful interactions between susceptible tumor cells and free viruses [3, 13, 31, 37, 41, 42].

The second term, $-\mu T_i$, represents the loss of infected tumor cells due to virus-induced lysis, where μ is the lysis rate. In line with standard assumptions in oncolytic virotherapy models, infected tumor cells are not assumed to proliferate, as viral replication rapidly leads to cell death [31]. Thus, no growth term is included for T_i. This reflects the short lifespan of infected cells and their primary role as virus-producing units[13, 37, 41, 42].

In Eq. (3.4), the dynamics of free oncolytic viruses V are modeled [3]. The first term, pT_i, represents the production of new virions from lysed infected tumor cells, where p denotes the viral burst size (i.e., the average number of virions released per lysed cell) [13, 31, 37].

The second term, $-\delta V$, accounts for the natural clearance or decay of free viruses in the tumor microenvironment, where δ is the viral decay rate [31]. This clearance may result from physical degradation, immune-mediated neutralization, or other nonspecific processes [13, 37].

In addition, following previous studies, external administration of oncolytic viruses can be incorporated via an impulsive source term of the form

$$\mu_v(t) = \mu_v(0)\Delta(t - \tau),$$

where $\mu_v(0)$ represents the dose of injected viruses at time τ, and $\Delta(\cdot)$ is the Dirac delta function. This formulation allows for modeling discrete viral injections at prescribed treatment times [43].

Overall, the model captures the interplay between susceptible and resistant tumor populations, viral infection dynamics, and density-dependent growth regulated by the Allee effect. The inclusion of the Allee effect introduces critical thresholds that can determine whether tumor populations persist or collapse, while the resistant population provides a mechanism for treatment failure or relapse [17, 44, 45]. The competition between these subpopulations, coupled with viral replication and clearance, governs the long-term outcomes of oncolytic virotherapy.

TABLE. 3.1. **Description of parameters involved in the model**

Parameter	Description
ρ_u	Proliferation rate of susceptible tumor cells
ρ_r	Proliferation rate of resistant tumor cells
K	Carrying capacity of total tumor population
β	Infection rate of susceptible tumor cells by free virus
μ	Lysis (death) rate of infected tumor cells
p	Viral burst size (virions released per lysed cell)
δ	Natural decay/clearance rate of free virus
α_s	Strong Allee effect threshold parameter
α_w	Weak Allee effect threshold parameter

TABLE. 3.2. **Model Parameters: Baseline Values and Ranges Used in Model Simulations**

Parameter	Baseline value	Range	Units	References
ρ_u	0.35	[0.12-1.20]	$(day)^{-1}$	[46, 47]
ρ_r	0.24	$[0-1]$	$(day)^{-1}$	[48]
K	1.04×10^8	$[10^7 - 10^9]$	$cells$	[46, 47]
β	1.0×10^{-9}	$[6.0 \times 10^{-12} - 0.862]$	$(PFU.day)^{-1}$	[39, 40]
μ	0.5	$[0.5 - 2.667]$	$(day)^{-1}$	[46, 47]
p	50	$[10 - 1350]$	$(PFU)(cell)^{-1}$	[39, 46, 47, 49]
δ	0.4	$[0.024 - 24]$	$(day)^{-1}$	[39, 46, 47, 49]
α_s	50	$\{50, 100, 150\}$	–	Estimated
α_w	20	$\{20, 2 \times 10^6, 2 \times 10^9\}$	–	Estimated

3.4 Boundedness of the Model

To ensure the proposed oncolytic virus model is biologically meaningful and mathematically well-posed, we must establish that all population variables remain non-negative and bounded for all time $t > 0$, given non-negative initial conditions [3].

Theorem 1 *Given the initial conditions $T_u(0) \geq 0$, $T_r(0) \geq 0$, $T_i(0) \geq 0$, and $V(0) \geq 0$, the solutions $(T_u(t), T_r(t), T_i(t), V(t))$ of the system (3.1)–(3.4) remain non-negative and*

bounded for all $t > 0$. *Furthermore, the region*

$$\Omega = \left\{ (T_u, T_r, T_i, V) \in \mathbb{R}^4_+ \;\middle|\; T_u + T_r + T_i \leq M_1,\ V \leq \frac{pM_1}{\delta} \right\} \tag{3.5}$$

is a positively invariant set for the system, where $M_1 = \max\{N(0), K\}$ *and* $N(t) = T_u(t) + T_r(t) + T_i(t)$.

Proof. Positivity: We first evaluate the vector field on the boundaries of the non-negative orthant $\mathbb{R}^4_+$:

$$\begin{aligned}
\left.\frac{dT_u}{dt}\right|_{T_u=0} &= 0 \geq 0, \\
\left.\frac{dT_r}{dt}\right|_{T_r=0} &= 0 \geq 0, \\
\left.\frac{dT_i}{dt}\right|_{T_i=0} &= \beta T_u V \geq 0 \quad (\text{since } T_u, V \geq 0), \\
\left.\frac{dV}{dt}\right|_{V=0} &= pT_i \geq 0 \quad (\text{since } T_i \geq 0).
\end{aligned}$$

Since the vector field points strictly inward or is tangent to the boundaries, $\mathbb{R}^4_+$ is a positively invariant set [50]. Thus, any trajectory starting with non-negative initial conditions remains non-negative for all $t > 0$.

Boundedness of the Tumor Population: Let $N(t) = T_u(t) + T_r(t) + T_i(t)$ denote the total tumor population. Differentiating $N(t)$ with respect to time and substituting the relevant equations yields,

$$\frac{dN}{dt} = \rho_u T_u \left(1 - \frac{N}{K}\right)\left(\frac{T_u - \alpha_s}{T_u + \alpha_w}\right) + \rho_r T_r \left(1 - \frac{N}{K}\right)\left(\frac{T_r - \alpha_s}{T_r + \alpha_w}\right) - \mu T_i.$$

Note that for any $T_j \geq 0$ (where $j \in \{u, r\}$), the Allee effect term satisfies the upper bound $\frac{T_j - \alpha_s}{T_j + \alpha_w} \leq 1$, under the standard biological assumption that $\alpha_s + \alpha_w > 0$. Let $\rho = \max\{\rho_u, \rho_r\}$. We can bound the total growth rate as,

$$\frac{dN}{dt} \leq \rho(T_u + T_r)\left(1 - \frac{N}{K}\right) - \mu T_i.$$

Consider the domain where $N(t) > K$. In this region, the logistic term $\left(1 - \frac{N}{K}\right) < 0$. Since we established $T_u, T_r \geq 0$, the sum $\rho(T_u + T_r)$ is non-negative, making the entire

growth term strictly negative. Furthermore, because $-\mu T_i \leq 0$, it follows that whenever $N(t) > K$, $\frac{dN}{dt} < 0$. By standard comparison theorems for ordinary differential equations [51], $N(t)$ cannot grow indefinitely and is bounded above by,

$$\limsup_{t\to\infty} N(t) \leq \max\{N(0), K\} := M_1. \tag{3.6}$$

Consequently, the individual sub-populations $T_u(t)$, $T_r(t)$, and $T_i(t)$ are strictly bounded by M_1.

Boundedness of the Viral Population: Using the established bound for infected cells, $T_i(t) \leq M_1$, we analyze the dynamics of the free virus population from Eq. (3.4),

$$\frac{dV}{dt} = pT_i - \delta V \leq pM_1 - \delta V.$$

This forms a first-order linear differential inequality. Applying Gronwall's inequality [52], we obtain,

$$V(t) \leq V(0)e^{-\delta t} + \frac{pM_1}{\delta}\left(1 - e^{-\delta t}\right).$$

Taking the limit as $t \to \infty$, the exponential decay terms vanish, yielding,

$$\limsup_{t\to\infty} V(t) \leq \frac{pM_1}{\delta}. \tag{3.7}$$

Since all state variables T_u, T_r, T_i, and V are strictly non-negative and bounded above by finite constants, the system is mathematically bounded in the invariant region Ω. This completes the proof. ■

3.5 Model analysis

3.5.1 Derivation of the steady states for the model without Allee effect

We find the steady states for the model without Allee effect by setting the population growth rates to zero.

$$\rho_u T_u \left(1 - \frac{T_u + T_r}{K}\right) - \beta T_u V = 0, \tag{3.8}$$

$$\rho_r T_r \left(1 - \frac{T_u + T_r}{K}\right) = 0, \tag{3.9}$$

$$\beta T_u V - \mu T_i = 0, \tag{3.10}$$

$$pT_i - \delta V = 0. \tag{3.11}$$

From Eq. (3.11), we express the virus population in terms of infected cells:

$$V = \frac{pT_i}{\delta}. \tag{3.12}$$

Substitution of Eq.(3.12) into Eq. (3.10) yields,

$$T_i \left(\frac{\beta p T_u}{\delta} - \mu\right) = 0. \tag{3.13}$$

This implies either $T_i = 0$ or $T_u = \frac{\delta\mu}{\beta p}$.

Case 1: $T_i = 0$ **(Infection-Free)**
If $T_i = 0$, then $V = 0$. Equations (3.8) and (3.9) become,

$$\rho_u T_u \left(1 - \frac{T_u + T_r}{K}\right) = 0,$$

$$\rho_r T_r \left(1 - \frac{T_u + T_r}{K}\right) = 0.$$

Extinction State $\mathcal{S}_0$: Setting $T_u = 0$ and $T_r = 0$,

$$\mathcal{S}_0 = (0, 0, 0, 0).$$

Uninfected Sensitive State $\mathcal{S}_1$: Setting $T_r = 0$ and $1 - \frac{T_u}{K} = 0$,

$$\mathcal{S}_1 = (K, 0, 0, 0).$$

Resistant-Only State $\mathcal{S}_2$: Setting $T_u = 0$ and $1 - \frac{T_r}{K} = 0$,

$$\mathcal{S}_2 = (0, K, 0, 0).$$

Tumor Coexistence $\mathcal{S}_3$: Setting $1 - \frac{T_u + T_r}{K} = 0$ (Line of equilibria),

$$\mathcal{S}_3 = (T_u, K - T_u, 0, 0).$$

Case 2: $T_u = \frac{\delta\mu}{\beta p}$ **(Active Infection)**
Substituting $T_u^* = \frac{\delta\mu}{\beta p}$ into Eq. (3.9), we find two subcases.

Infected-Resistant Boundary $\mathcal{S}_4$: If $1 - \frac{T_u + T_r}{K} = 0$, then $T_r = K - \frac{\delta\mu}{\beta p}$.

Substituting this back into Eq. (3.8) forces $V = 0$ (and thus $T_i = 0$),

$$\mathcal{S}_4 = \left(\frac{\delta\mu}{\beta p}, K - \frac{\delta\mu}{\beta p}, 0, 0\right), \text{ for } \mathcal{R}_0 > 1.$$

Virotherapy Steady State $\mathcal{S}_5$: If $T_r = 0$, Eq. (3.8) becomes, $\rho_u \frac{\delta\mu}{\beta p}\left(1 - \frac{\delta\mu}{K\beta p}\right) = \beta \frac{\delta\mu}{\beta p} V$.

Solving for V and T_i using $T_i = \frac{\delta V}{p}$,

$$\mathcal{S}_5 = \left(\frac{\delta\mu}{\beta p}, 0, \frac{\delta\rho_u(K\beta p - \delta\mu)}{K\beta^2 p^2}, \frac{\rho_u(K\beta p - \delta\mu)}{K\beta^2 p}\right), \text{ for } \mathcal{R}_0 > 1.$$

3.5.2 Calculation of the Basic Reproduction Number ($\mathcal{R}_0$)

The basic reproduction number is calculated using the Next-Generation Matrix method at the infection-free steady state $\mathcal{S}_1 = (K, 0, 0, 0)$.

Infection and Transition Rate Vectors

To apply the Next-Generation Matrix method, we first express the infected subsystem (T_i, V) in the form $\dot{x} = \mathcal{F}(x) - \mathcal{V}(x)$. The vector $\mathcal{F}$ represents the rate of appearance of new infections, and $\mathcal{V}$ represents the rate of transfer of individuals (or virions) out of or between infected compartments [37, 53, 54].

For our system, these vectors are

$$\mathcal{F} = \begin{pmatrix} \beta T_u V \\ 0 \end{pmatrix}, \quad \mathcal{V} = \begin{pmatrix} \mu T_i \\ -pT_i + \delta V \end{pmatrix} \tag{3.14}$$

where,

$\beta T_u V$ is the rate at which new infected tumor cells are created.

μT_i is the death rate of infected tumor cells.

$-pT_i$ represents the production of new virions by infected cells (a transition into the V compartment).δV is the clearance rate of free virions.

Infected Subsystem We consider the compartments representing the infection: $x = (T_i, V)^T$. The rates of new infection $(\mathcal{F})$ and the rates of transfer $(\mathcal{V})$ are

$$\mathcal{F} = \begin{bmatrix} 0 & \beta K \\ 0 & 0 \end{bmatrix}, \quad \mathcal{V} = \begin{bmatrix} \mu & 0 \\ -p & \delta \end{bmatrix}.$$

3.5.3 Next-Generation Matrix

The next-generation matrix is defined as $K = \mathcal{F}\mathcal{V}^{-1}$. First, we find $\mathcal{V}^{-1}$ as,

$$\mathcal{V}^{-1} = \begin{bmatrix} \frac{1}{\mu} & 0 \\ \frac{p}{\mu\delta} & \frac{1}{\delta} \end{bmatrix}.$$

Multiplying gives,

$$K = \begin{bmatrix} \frac{\beta K p}{\mu\delta} & \frac{\beta K}{\delta} \\ 0 & 0 \end{bmatrix}.$$

Final $\mathcal{R}_0$ Expression

The reproduction number is the spectral radius (dominant eigenvalue) of K [54]:

$$\mathcal{R}_0 = \frac{\beta K p}{\mu \delta}. \tag{3.15}$$

The virus can only persist in the tumor population if $\mathcal{R}_0 > 1$ [37, 53, 54].

3.5.4 Stability Analysis of the Extinction State $\mathcal{S}_0$

The extinction state is defined as $\mathcal{S}_0 = (0, 0, 0, 0)$. To determine its stability, we compute the Jacobian matrix J of the system.

$$J = \begin{pmatrix} \frac{\partial f_1}{\partial T_u} & \frac{\partial f_1}{\partial T_r} & \frac{\partial f_1}{\partial T_i} & \frac{\partial f_1}{\partial V} \\ \frac{\partial f_2}{\partial T_u} & \frac{\partial f_2}{\partial T_r} & \frac{\partial f_2}{\partial T_i} & \frac{\partial f_2}{\partial V} \\ \frac{\partial f_3}{\partial T_u} & \frac{\partial f_3}{\partial T_r} & \frac{\partial f_3}{\partial T_i} & \frac{\partial f_3}{\partial V} \\ \frac{\partial f_4}{\partial T_u} & \frac{\partial f_4}{\partial T_r} & \frac{\partial f_4}{\partial T_i} & \frac{\partial f_4}{\partial V} \end{pmatrix}. \tag{3.16}$$

Evaluation at $\mathcal{S}_0$: Evaluating the partial derivatives at $(0, 0, 0, 0)$ we get,

$$\left.\frac{\partial f_1}{\partial T_u}\right|_{(0,0,0,0)} = \left[\rho_u(1 - \frac{2T_u + T_r}{K}) - \beta V\right]\Bigg|_{(0,0,0,0)} = \rho_u$$
$$\left.\frac{\partial f_2}{\partial T_r}\right|_{(0,0,0,0)} = \left[\rho_r(1 - \frac{T_u + 2T_r}{K})\right]\Bigg|_{(0,0,0,0)} = \rho_r.$$

Other terms like $\dfrac{\partial f_1}{\partial T_r}$ and $\dfrac{\partial f_3}{\partial T_u}$ vanish at the origin.

The Jacobian at $\mathcal{S}_0$ is

$$J(\mathcal{S}_0) = \begin{pmatrix} \rho_u & 0 & 0 & 0 \\ 0 & \rho_r & 0 & 0 \\ 0 & 0 & -\mu & 0 \\ 0 & 0 & p & -\delta \end{pmatrix}. \tag{3.17}$$

The eigenvalues are the roots of the characteristic equation $|J(\mathcal{S}_0) - \lambda I| = 0$. Because the

matrix is block diagonal, the eigenvalues are,

$$\lambda_1 = \rho_u,$$
$$\lambda_2 = \rho_r,$$
$$\lambda_3 = -\mu,$$
$$\lambda_4 = -\delta.$$

Since $\rho_u > 0$ and $\rho_r > 0$, there exist at least two positive eigenvalues. Therefore, the extinction state $\mathcal{S}_0$ is unstable [55]. Biologically, this means that if a small number of tumor cells are introduced, the population will grow rather than die out [56].

3.5.5 Stability Analysis of the Uninfected Tumor State $\mathcal{S}_1$

The uninfected state is $\mathcal{S}_1 = (K, 0, 0, 0)$. The Jacobian matrix evaluated at this point is

$$J(\mathcal{S}_1) = \begin{pmatrix} -\rho_u & -\rho_u & 0 & -\beta K \\ 0 & 0 & 0 & 0 \\ 0 & 0 & -\mu & \beta K \\ 0 & 0 & p & -\delta \end{pmatrix}. \tag{3.18}$$

The eigenvalues are found from the characteristic equation $\det(J(\mathcal{S}_1) - \lambda I) = 0$

$$(-\rho_u - \lambda)(-\lambda)\left[(-\mu - \lambda)(-\delta - \lambda) - \beta K p\right] = 0. \tag{3.19}$$

The first two eigenvalues are

$$\lambda_1 = -\rho_u < 0, \tag{3.20}$$
$$\lambda_2 = 0 \quad \text{(Neutral stability due to the presence of } T_r \text{ in the model).} \tag{3.21}$$

The remaining eigenvalues $\lambda_{3,4}$ are found from the infection sub-block

$$\lambda^2 + (\mu + \delta)\lambda + (\mu\delta - p\beta K) = 0 \tag{3.22}$$

as

$$\lambda_{3,4} = \frac{-(\mu + \delta) \pm \sqrt{(\mu + \delta)^2 - 4(\mu\delta - p\beta K)}}{2}. \tag{3.23}$$

By defining the basic reproduction number as $R_0 = \frac{p\beta K}{\mu\delta}$, the Equation (3.22) becomes

$$\lambda^2 + (\mu + \delta)\lambda + \mu\delta(1 - R_0) = 0. \tag{3.24}$$

Thus, the corresponding eigenvalues are

$$\lambda_{3,4} = \frac{-(\mu + \delta) \pm \sqrt{(\mu + \delta)^2 - 4\mu\delta(1 - R_0)}}{2}. \tag{3.25}$$

Note that if $R_0 > 1$, the constant term $\mu\delta(1 - R_0)$ becomes negative, ensuring one positive real eigenvalue and making $\mathcal{S}_1$ unstable.

1. According to the Routh-Hurwitz criteria, for the roots of the quadratic to have negative real parts, all coefficients must be positive [57].

$$(\mu + \delta) > 0 \qquad \text{(Always satisfied)}. \tag{3.26}$$

$$\mu\delta(1 - \mathcal{R}_0) > 0 \implies \mathcal{R}_0 < 1. \tag{3.27}$$

   Therefore, if $\mathcal{R}_0 < 1$, the virus will die out, and the state is locally stable (ignoring the neutral T_r direction). If $\mathcal{R}_0 > 1$, the uninfected tumor state is unstable, and the infection will spread [55, 56].

2. When $\lambda_2 = 0$, the equilibrium $\mathcal{S}_1$ is non-hyperbolic. This zero eigenvalue corresponds to the eigenvector in the T_r direction, indicating a line of equilibria defined by $T_u + T_r = K$ [58].

   (a) **Mathematical Stability:** The system is *marginally stable*. Small perturbations along the T_r axis result in the system settling into a new equilibrium on the line $T_u + T_r = K$ rather than returning to $\mathcal{S}_1$ [59].

   (b) **Biological Meaning:** This represents a state of niche saturation where uninfected and resistant cells occupy the same ecological space. Without a specific birth/death advantage ($\rho_u = \rho_r$), the population ratio is determined solely by initial conditions.

3.5.6 Stability Analysis of $\mathcal{S}_2 = (0, K, 0, 0)$

The Jacobian matrix evaluated at the resistant-only state $\mathcal{S}_2$ is

$$J(\mathcal{S}_2) = \begin{pmatrix} 0 & 0 & 0 & 0 \\ -\rho_r & -\rho_r & 0 & 0 \\ 0 & 0 & -\mu & 0 \\ 0 & 0 & p & -\delta \end{pmatrix}. \tag{3.28}$$

The eigenvalues are $\lambda_1 = 0, \lambda_2 = -\rho_r, \lambda_3 = -\mu$, and $\lambda_4 = -\delta$.

Because $\lambda_1 = 0$ and all other eigenvalues are negative, $\mathcal{S}_2$ is marginally stable. Biologically, this state is resistant to viral invasion because the target cell population T_u is extinct, leaving no fuel for the infection to propagate.

3.5.7 The Coexistence State $\mathcal{S}_3$

The tumor coexistence state, or the line of equilibria, is defined by the condition where the total cell population reaches the carrying capacity K in the absence of infection ($T_i = 0, V = 0$). This state is represented by,

$$\mathcal{S}_3 = (T_u, K - T_u, 0, 0) \quad \text{for} \quad T_u \in (0, K). \tag{3.29}$$

To determine the local stability of $\mathcal{S}_3$, we evaluate the Jacobian matrix of the system at this point. By substituting $T_r = K - T_u$ and $1 - \frac{T_u + T_r}{K} = 0$, the Jacobian simplifies to

$$J(\mathcal{S}_3) = \begin{pmatrix} -\frac{\rho_u T_u}{K} & -\frac{\rho_u T_u}{K} & 0 & -\beta T_u \\ -\frac{\rho_r (K - T_u)}{K} & -\frac{\rho_r (K - T_u)}{K} & 0 & 0 \\ 0 & 0 & -\mu & \beta T_u \\ 0 & 0 & p & -\delta \end{pmatrix}. \tag{3.30}$$

The characteristic equation $\det(J(\mathcal{S}_3) - \lambda I) = 0$ is block-triangular, allowing us to solve for the eigenvalues in two distinct pairs.

The first two eigenvalues are derived from the upper-left 2×2 block,

$$\det \begin{pmatrix} -\frac{\rho_u T_u}{K} - \lambda & -\frac{\rho_u T_u}{K} \\ -\frac{\rho_r (K - T_u)}{K} & -\frac{\rho_r (K - T_u)}{K} - \lambda \end{pmatrix} = \lambda^2 + \left(\frac{\rho_u T_u + \rho_r (K - T_u)}{K} \right) \lambda = 0. \tag{3.31}$$

The eigenvalues are

- $\lambda_1 = 0$. Indicates *marginal (neutral) stability.* Because $\mathcal{S}_3$ is a line of equilibria, any perturbation along the line $T_u + T_r = K$ results in a shift to a new equilibrium point rather than a return to the original state.
- $\lambda_2 = -\frac{\rho_u T_u + \rho_r (K - T_u)}{K}$. Since $\rho_u, \rho_r, T_u, K > 0$, this eigenvalue is always negative, representing the stability of the total population size relative to the carrying capacity K.

The remaining two eigenvalues determine whether a viral introduction will grow or decay.

$$\lambda^2 + (\mu + \delta)\lambda + \mu\delta \left(1 - \mathcal{R}_0 \frac{T_u}{K}\right) = 0, \tag{3.32}$$

where $\mathcal{R}_0 = \frac{p\beta K}{\mu\delta}$. The eigenvalues $\lambda_{3,4}$ are

$$\lambda_{3,4} = \frac{-(\mu + \delta) \pm \sqrt{(\mu + \delta)^2 - 4\mu\delta(1 - \mathcal{R}_0 \frac{T_u}{K})}}{2}. \tag{3.33}$$

The stability of the coexistence state is contingent on the effective density of uninfected cells T_u.

- **Infection Suppression:** If $\mathcal{R}_0 \frac{T_u}{K} < 1$, then $\lambda_{3,4}$ have negative real parts. In this regime, the viral load V and infected cells T_i will decay to zero. This shows that even if the virus could infect a full tumor ($\mathcal{R}_0 > 1$), a sufficiently high proportion of resistant cells (T_r) can lower the target cell density (T_u) enough to stop the spread.
- **Viral Outbreak:** If $\mathcal{R}_0 \frac{T_u}{K} > 1$, then $\lambda_3 > 0$. The state $\mathcal{S}_3$ becomes unstable, and the introduction of a virus will lead to an epidemic within the uninfected cell population.

3.5.8 The Viral Threshold State $\mathcal{S}_4$

The resistant dominance state, denoted as $\mathcal{S}_4$, represents the specific equilibrium where the uninfected tumor cell population is maintained exactly at the threshold required for

viral persistence, while the resistant cells fill the remaining carrying capacity. This state is defined by:

$$\mathcal{S}_4 = \left(\frac{\delta\mu}{\beta p}, K - \frac{\delta\mu}{\beta p}, 0, 0\right). \tag{3.34}$$

For this state to exist within the physical domain ($T_r > 0$), the condition $K > \frac{\delta\mu}{\beta p}$ must be satisfied, which is equivalent to the basic reproduction number $\mathcal{R}_0 = \frac{p\beta K}{\mu\delta}$ being greater than unity.

To evaluate the local stability of $\mathcal{S}_4$, we define $T_u^* = \frac{\delta\mu}{\beta p}$ and $T_r^* = K - T_u^*$. Substituting these values along with $T_i = 0$ and $V = 0$ into the general Jacobian matrix, we observe that the term $1 - \frac{T_u+T_r}{K}$ vanishes since $T_u^* + T_r^* = K$. The Jacobian simplifies to

$$J(\mathcal{S}_4) = \begin{pmatrix} -\frac{\rho_u T_u^*}{K} & -\frac{\rho_u T_u^*}{K} & 0 & -\beta T_u^* \\ -\frac{\rho_r T_r^*}{K} & -\frac{\rho_r T_r^*}{K} & 0 & 0 \\ 0 & 0 & -\mu & \beta T_u^* \\ 0 & 0 & p & -\delta \end{pmatrix}. \tag{3.35}$$

The block-triangular structure of $J(\mathcal{S}_4)$ allows the characteristic equation $\det(J(\mathcal{S}_4) - \lambda I) = 0$ to be partitioned into two independent quadratic factors.

The first pair of eigenvalues is obtained from the upper-left 2×2 sub-matrix whose determinant is

$$\det\begin{pmatrix} -\frac{\rho_u T_u^*}{K} - \lambda & -\frac{\rho_u T_u^*}{K} \\ -\frac{\rho_r T_r^*}{K} & -\frac{\rho_r T_r^*}{K} - \lambda \end{pmatrix} = \lambda^2 + \left(\frac{\rho_u T_u^* + \rho_r T_r^*}{K}\right)\lambda = 0. \tag{3.36}$$

The first eigenvalue, $\lambda_1 = 0$, indicates that the system possesses marginal stability, reflecting the fact that $\mathcal{S}_4$ lies on a continuum of steady states where $T_u + T_r = K$. The second eigenvalue, $\lambda_2 = -\frac{\rho_u T_u^* + \rho_r T_r^*}{K}$, is strictly negative for all positive parameters, signifying that the total tumor volume is stable and returns to the carrying capacity K following small perturbations in size.

The stability of the viral components is governed by the lower-right 2×2 sub-matrix whose determinant is

$$\det\begin{pmatrix} -\mu - \lambda & \beta T_u^* \\ p & -\delta - \lambda \end{pmatrix} = \lambda^2 + (\mu + \delta)\lambda + (\mu\delta - \beta p T_u^*) = 0. \tag{3.37}$$

Substituting $T_u^* = \frac{\delta\mu}{\beta p}$ into the constant term results in $\mu\delta - \beta p(\frac{\delta\mu}{\beta p}) = 0$. Consequently, the characteristic equation reduces to $\lambda^2 + (\mu + \delta)\lambda = 0$, yielding eigenvalues $\lambda_3 = 0$ and

$\lambda_4 = -(\mu + \delta)$.

Therefore eigenvlues are

$$\begin{aligned}
\lambda_1 &= 0, \\
\lambda_2 &= -\frac{\rho_u T_u^* + \rho_r T_r^*}{K} < 0, \\
\lambda_3 &= 0, \\
\lambda_4 &= -(\mu + \delta) < 0.
\end{aligned}$$

The stability analysis reveals that $\mathcal{S}_4$ is a non-hyperbolic equilibrium point due to the presence of two zero eigenvalues ($\lambda_1 = \lambda_3 = 0$). Biologically, this state represents the transcritical bifurcation point where the effective reproduction number $\mathcal{R}_e = \mathcal{R}_0 \frac{T_u^*}{K}$ [60], defined as the quantity of individuals within a population that can be infected by a single person at any given moment [60, 61], is exactly equal to one. While the negative eigenvalues λ_2 and λ_4 ensure that the system converges toward the tumor carrying capacity and the viral threshold, the zero eigenvalues signify that $\mathcal{S}_4$ is the critical boundary between viral extinction and a viral outbreak. For $\mathcal{R}_0 > 1$, this state is essentially the "tipping point" where any shift in the ratio of uninfected to resistant cells will determine the success of the virotherapy.

3.5.9 The Endemic Equilibrium State $\mathcal{S}_5$

The endemic equilibrium $\mathcal{S}_5$ represents a steady state where the virus and uninfected tumor cells coexist, while the resistant tumor cell population is completely absent ($T_r = 0$). This state is defined by the coordinates:

$$\mathcal{S}_5 = \left(\frac{\delta\mu}{\beta p}, 0, \frac{\delta\rho_u(K\beta p - \delta\mu)}{K\beta^2 p^2}, \frac{\rho_u(K\beta p - \delta\mu)}{K\beta^2 p} \right). \tag{3.38}$$

By utilizing the basic reproduction number $\mathcal{R}_0 = \frac{p\beta K}{\mu\delta}$, the components can be expressed as $T_u^* = \frac{K}{\mathcal{R}_0}$, $T_i^* = \frac{\rho_u \delta}{\beta p \mathcal{R}_0}(\mathcal{R}_0 - 1)$, and $V^* = \frac{\rho_u}{\beta \mathcal{R}_0}(\mathcal{R}_0 - 1)$. For $\mathcal{S}_5$ to be biologically feasible, the condition $\mathcal{R}_0 > 1$ must be satisfied to ensure positive population densities.

The Jacobian Matrix To determine the local stability of $\mathcal{S}_5$, we evaluate the Jacobian matrix of the system at this equilibrium point. Note that at $\mathcal{S}_5$, the infection term $\beta T_u^* V^*$ exactly balances the logistic growth of the uninfected cells, such that $\rho_u(1 - \frac{T_u^*}{K}) = \beta V^*$. The Jacobian simplifies to:

$$J(\mathcal{S}_5) = \begin{pmatrix} -\frac{\rho_u T_u^*}{K} - \beta V^* & -\frac{\rho_u T_u^*}{K} & 0 & -\beta T_u^* \\ 0 & \rho_r(1 - \frac{T_u^*}{K}) & 0 & 0 \\ \beta V^* & 0 & -\mu & \beta T_u^* \\ 0 & 0 & p & -\delta \end{pmatrix}. \tag{3.39}$$

The structure of $J(\mathcal{S}_5)$ is partially block-triangular, allowing us to immediately extract one eigenvalue from the second row and column.

The first eigenvalue is associated with the resistant cell compartment T_r,

$$\lambda_1 = \rho_r \left(1 - \frac{T_u^*}{K}\right) = \rho_r \left(1 - \frac{1}{\mathcal{R}_0}\right). \tag{3.40}$$

Since we assume $\mathcal{R}_0 > 1$ and $\rho_r > 0$, it follows that $\lambda_1 > 0$. This positive eigenvalue indicates that the state $\mathcal{S}_5$ is unstable in the presence of resistant cells.

The remaining three eigenvalues are derived from the 3×3 sub-matrix involving T_u, T_i, and V:

$$\det \begin{pmatrix} -\frac{\rho_u T_u^*}{K} - \beta V^* - \lambda & 0 & -\beta T_u^* \\ \beta V^* & -\mu - \lambda & \beta T_u^* \\ 0 & p & -\delta - \lambda \end{pmatrix} = 0. \tag{3.41}$$

This yields a characteristic polynomial of the form $P(\lambda) = \lambda^3 + A\lambda^2 + B\lambda + C = 0$. For the subsystem to be stable, the Routh-Hurwitz criteria require $A, C > 0$ and $AB > C$. Given $T_u^*, T_i^*, V^* > 0$, these conditions are generally satisfied, implying the (T_u, T_i, V) interaction is internally stable.

Therefore, the eigenvalues are

$$\lambda_1 = \rho_r \left(1 - \frac{1}{\mathcal{R}_0}\right) > 0,$$

$$\lambda_{2,3,4} = \text{Roots of } \lambda^3 + A\lambda^2 + B\lambda + C = 0 \text{ (with negative real parts)}.$$

The stability analysis demonstrates that $\mathcal{S}_5$ is an unstable saddle point when $\mathcal{R}_0 > 1$. Biologically, while the virus can effectively regulate the uninfected tumor cell population

at a steady endemic level, this very reduction in T_u reduces competition for the resistant cells. Because $\lambda_1 > 0$, any introduction of resistant cells will lead to their exponential growth, as they are not subject to viral predation and can exploit the niche space created by the viral reduction of uninfected cells. This suggests that without additional treatment to target the resistant population, the system will eventually transition from $\mathcal{S}_5$ toward a state where resistant cells dominate, such as $\mathcal{S}_4$.

3.6 Simulations

3.6.1 Model Dynamics without Allee effect

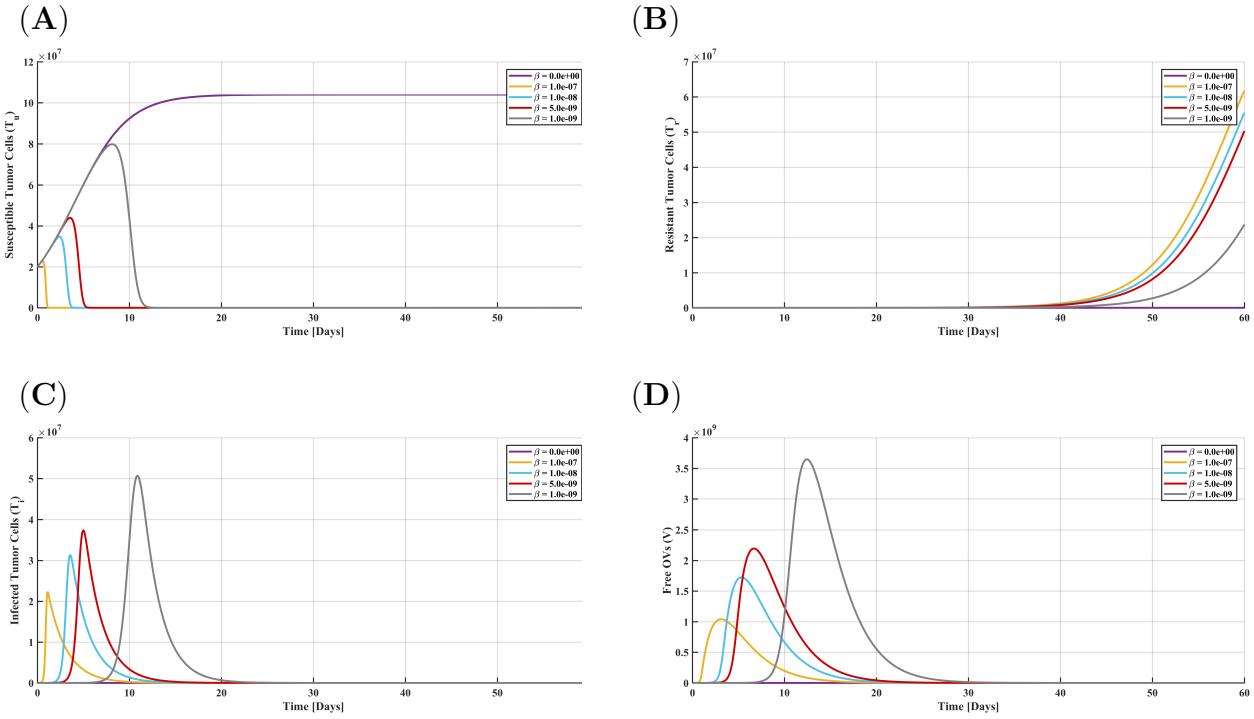

FIG. 3.2. **Model dynamics without Allee effect during OVT.**

(A) shows Uninfected tumor cell population progression, (B) resistant tumor cell population, (C) infected tumor cell population, and (D) free oncolytic virus (OV) concentration. All panels show system trajectories obtained by varying the infection rate β, ($\beta = 0$, 1.0×10^{-9}, 5.0×10^{-9}, 1.0×10^{-8}, 1.0×10^{-7} pfu^{-1} day^{-1}) while all other parameters remain at their baseline values in **Tab.** 3.2.

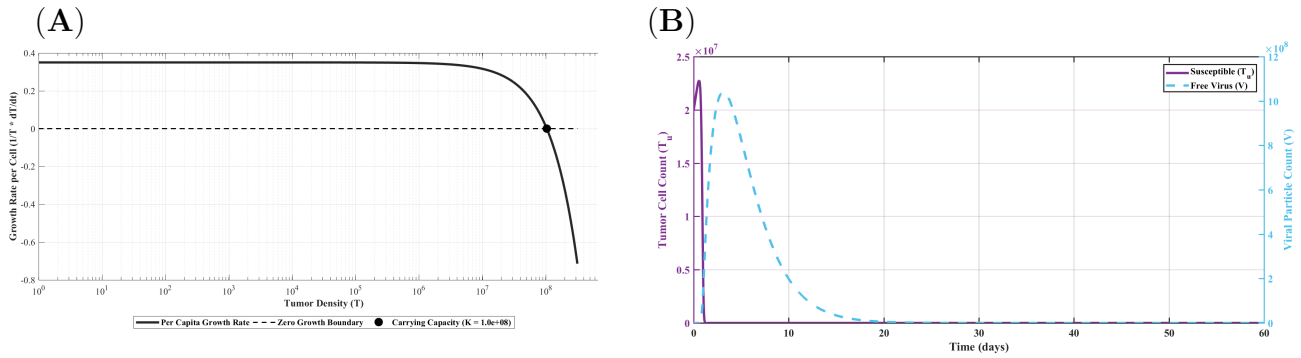

FIG. 3.3. **Phase potrait and $Tu - V$ Lag Analysis of the model without Allee effect.**

The findings shown in Figure 3.2 demonstrate how changing the infection rate β affects the model's dynamics without the Allee effect. The infection rate is a key factor that impacts how effectively free oncolytic viruses infect susceptible tumor cells. As β increases, the interaction between the virus and tumor cells becomes stronger, leading to major changes in the system's behavior [41].

Figure 3.2(A) shows the dynamics of the susceptible tumor cell population. At $\beta = 0$, there is no infection, and susceptible tumor cells grow quickly until they reach the carrying capacity. This represents uncontrolled tumor growth in the absence of viral infection. As β rises, the number of susceptible tumor cells decreases more quickly because more cells become infected by the virus. With high infection rates, the population of susceptible tumor cells is almost completely wiped out in a short time, which shows that higher values of β improve the therapy's effectiveness [4, 41, 62, 63].

Figure 3.2(B) illustrates the population of resistant tumor cells. When $\beta = 0$, the resistant population is very small. However, as β increases, the number of resistant cells grows gradually and eventually dominates the population. This happens because the removal of susceptible tumor cells creates space and resources for the resistant cells to expand. The results suggest that while higher infection rates reduce susceptible tumor cells, they may also support the rise and growth of resistant tumor populations [10, 41, 64, 65].

Figure 3.2(C) depicts the infected tumor cell population. For positive values of β, the infected cells grow rapidly, reach a peak, and then decline to zero. Higher infection rates

produce larger peaks since more susceptible tumor cells are infected in a shorter time. The decline is due to viral-induced cell death and the exhaustion of susceptible target cells. When $\beta = 0$, the infected population remains nonexistent throughout the simulation because there is no infection [4, 41, 62, 63].

Figure 3.2(D) shows the behavior of free oncolytic viruses. At first, the virus population increases as infected tumor cells release new viral particles through cell death. Higher values of β result in larger viral peaks because of more effective infection spread. However, once the susceptible tumor cells are depleted, the virus concentration drops quickly due to the lack of host cells needed for viral replication [4, 41, 62, 63].

Figure 3.3(A) presents the phase portrait of the model without the Allee effect. The per-capita growth rate stays positive at low tumor densities, only decreasing as it nears carrying capacity. This means that even small tumor populations can continue to grow, showing that natural extinction of tumors at low densities is unlikely without the Allee effect [13, 66].

Figure 3.3(B) illustrates the time delay between susceptible tumor cells and free viruses. The virus population sees a rapid increase after the infection starts, while the susceptible tumor cells experience a decline soon after. The time lag between viral growth and the decrease in tumor cells indicates the period needed for viral replication and cell death. As susceptible tumor cells are used up, the virus population also falls due to the lack of host cells to support viral replication [4, 41].

In conclusion, the findings suggest that increasing the infection rate β boosts the effectiveness of viral infection and leads to the destruction of susceptible tumor cells [4, 41, 62]. However, the absence of the Allee effect allows resistant tumor cells to survive and grow even after significant viral activity [41, 65]. This indicates that simply improving infection efficiency may not be enough for complete tumor eradication [67].

3.6.2 Model dynamics with Allee effect

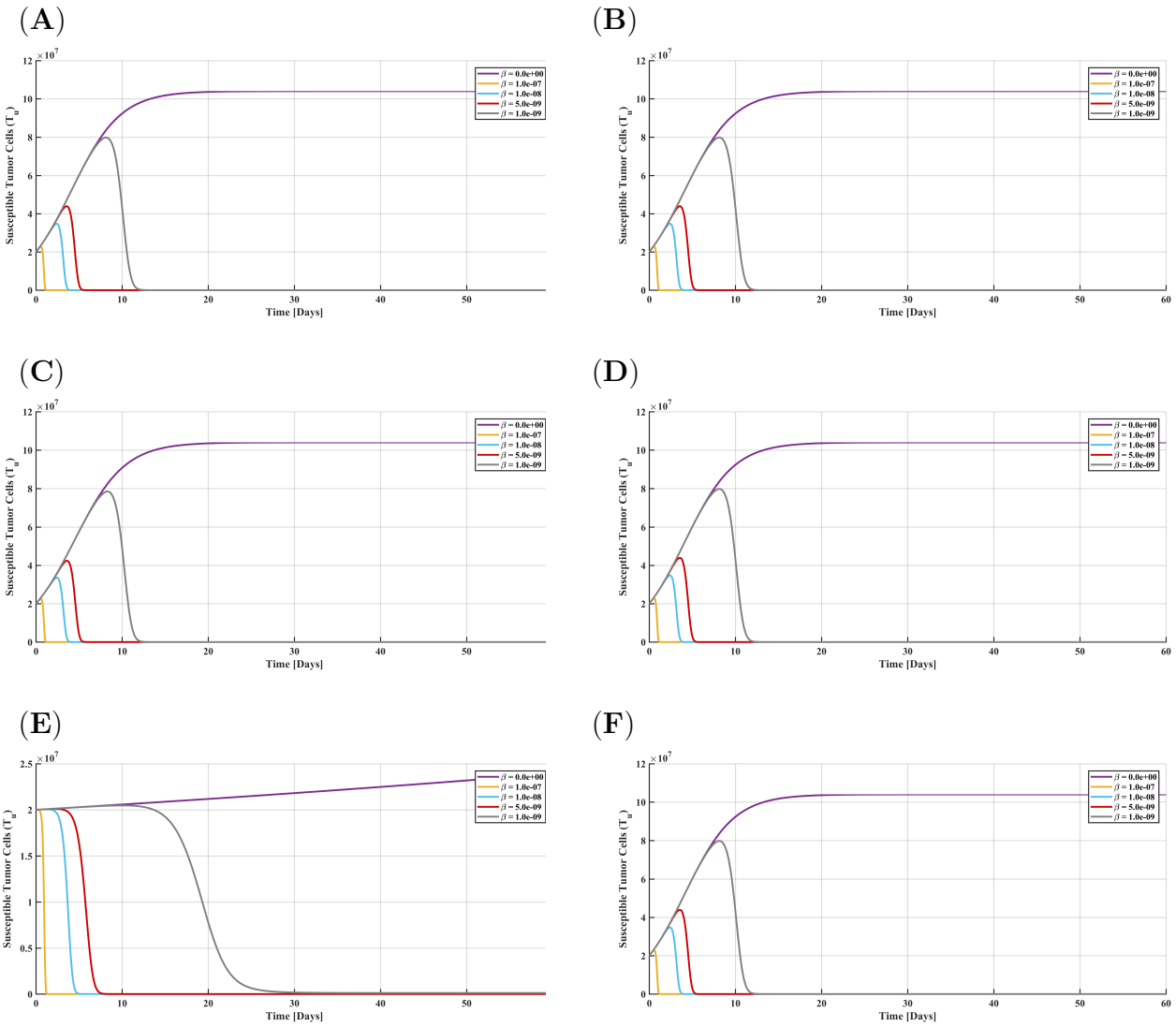

FIG. 3.4. **Allee effect on uninfected tumor cell population during OVT.**

(A),(C), and (E) illustrate the plots of the uninfected tumor cell population progression in the presence of weak Allee effect thresholds of $\alpha_w = 20,\ 2 \times 10^6, \text{and}\ 2 \times 10^9$ respectively. Similarly, (B),(D), and (F) show the plots of the uninfected tumor cell population dynamics in the presence of strong Allee effect thresholds of $\alpha_s = 50,\ 100, \text{and}\ 150$ respectively. All plots display the system trajectories obtained by varying the infection rate β, ($\beta = 0,\ 1.0 \times 10^{-9},\ 5.0 \times 10^{-9},\ 1.0 \times 10^{-8},\ 1.0 \times 10^{-7}$ pfu^{-1} day^{-1}), in addition to varying Allee effect parameters while other parameters remain at their baseline values in **Tab.** 3.2.

Figure 3.4 shows how both weak and strong Allee effects impact the population of uninfected tumor cells (T_u) during oncolytic virus therapy. In all simulations, a higher viral infection rate β speeds up the decline and eventual elimination of susceptible tumor cells. Without therapy ($\beta = 0$), the tumor can grow unchecked [4, 41, 62, 63].

In the case of a weak Allee effect, which has lower thresholds (as seen in panels A and C), the tumor grows rapidly without treatment and is quickly destroyed after viral administration.

When the weak Allee threshold is raised significantly to $\alpha_w = 2.0 \times 10^9$ (displayed in panel E), the tumor's baseline growth is greatly hindered because the initial tumor load is far below this threshold. This slowdown in growth leads to a slight delay in completely clearing the tumor at the lowest non-zero infection rate ($\beta = 1.0 \times 10^{-9}$ pfu^{-1} day^{-1}) [13, 17, 33]. The slow tumor growth results in fewer susceptible cells available for rapid viral replication [4].

In contrast, panels B, D, and F examine the system with a strong Allee effect, featuring thresholds of 50, 100, and 150. Since these thresholds are very low compared to the initial tumor volume of 2.0×10^7 cells, they have a minimal effect on the observable population trend. The main significance of the strong Allee effect in these cases occurs at the microscopic level. When the oncolytic virus successfully reduces the number of uninfected cells below these critical thresholds, the strong Allee effect guarantees the tumor's inevitable extinction, eliminating the possibility of a tumor rebound [13, 17, 33].

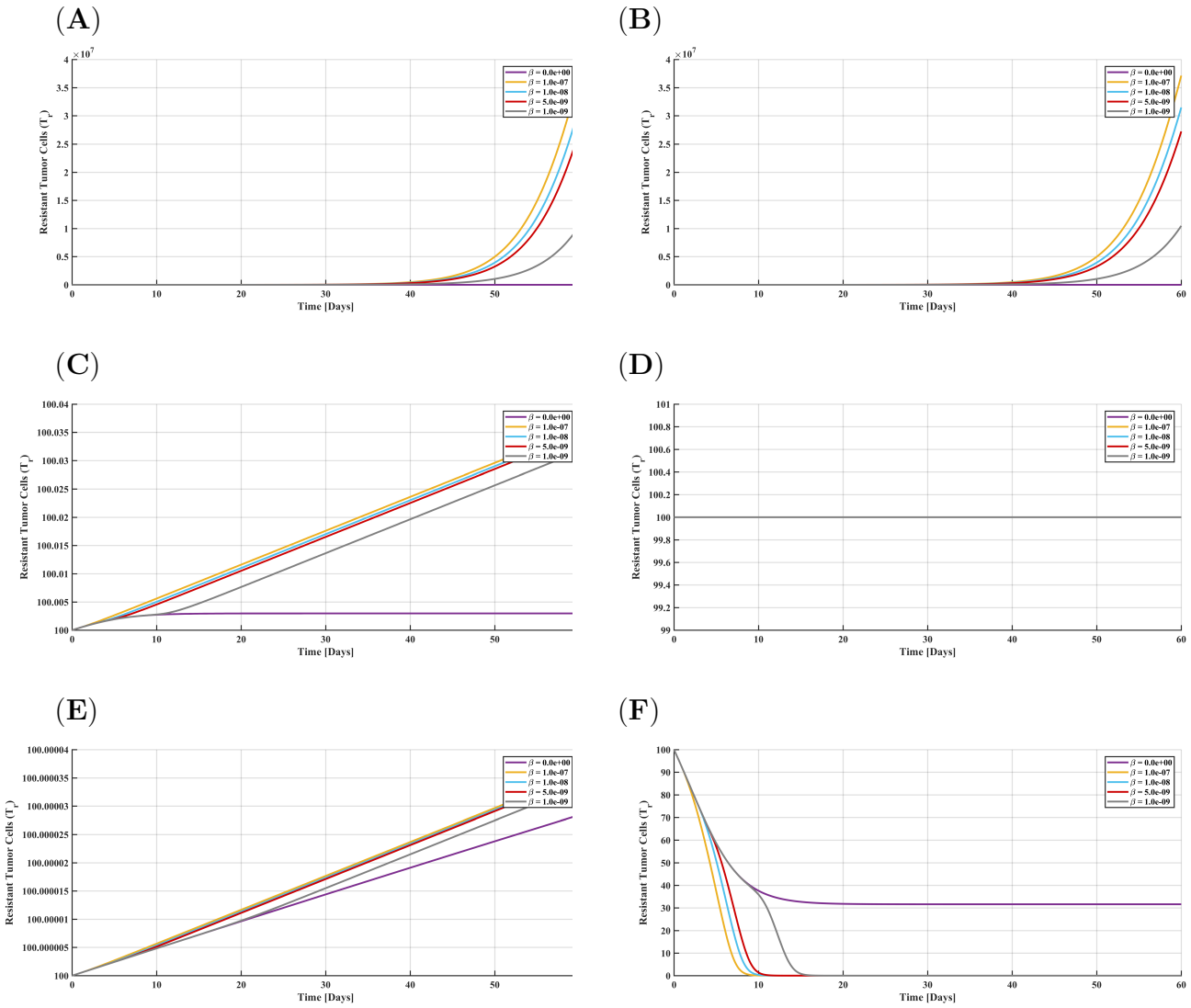

FIG. 3.5. **Allee effect on reistant tumor cell population during OVT.**

(A),(C), and (E) represent the plots of the resistant tumor cell population dynamics in the presence of weak Allee effect thresholds of $\alpha_w = 20,\ 2 \times 10^6,$ and 2×10^9 respectively. Similarly, (B),(D), and (F) illustrate the plots of the resistant tumor cell population dynamics in the presence of strong Allee effect thresholds of $\alpha_s = 50,\ 100,$ and 150 respectively. All plots display the system trajectories obtained by varying the infection rate β, ($\beta = 0,\ 1.0 \times 10^{-9},\ 5.0 \times 10^{-9},\ 1.0 \times 10^{-8},\ 1.0 \times 10^{-7}$ pfu^{-1} day^{-1}), in addition to varying Allee effect parameters while other parameters in **Tab.** 3.2 remain at their baseline values.

Figure 3.5 investigates the dynamics of the resistant tumor cell population (T_r) in relation to varying Allee effect thresholds and viral infection rates. A notable biological phenomenon that emerges in situations with low Allee thresholds (as seen in panels A and B) is competitive release [65, 68]. Surprisingly, as the viral infection rate β rises, the ultimate population of resistant tumor cells also increases. This occurs because the oncolytic virus effectively targets and eliminates the susceptible uninfected cells, which inadvertently reduces spatial and nutritional competition within the tumor microenvironment. The resulting availability of resources enables the resistant strain to proliferate vigorously [10, 41, 64, 65, 65]. In these particular instances, both the weak ($\alpha_w = 20$) and strong ($\alpha_s = 50$) Allee thresholds are insufficient to impede the swift emergence and exponential growth of the resistant cells.

In contrast, panels C and E reveal that the implementation of a significant weak Allee threshold ($\alpha_w = 2.0\times10^6$ and 2.0×10^9 , respectively) severely restricts the growth potential of the resistant population. Although OVT effectively removes the competing uninfected cells, the inherent proliferation penalty associated with the elevated weak Allee threshold keeps the resistant population relatively stagnant. The resulting microscopic increases in the resistant cell count lack substantial macroscopic significance, indicating that if a resistant strain is subjected to a high weak Allee effect, the clinical risk of competitive release following virotherapy is significantly reduced [13, 17, 33].

The unique regulatory influence of the strong Allee effect is most apparent in panels D and F. In panel D, the strong threshold of $\alpha_s = 100$ seems to perfectly balance the initial size of the resistant population, depriving the cells of the critical mass necessary for positive growth and leading to a completely stagnant, flat trajectory. More importantly, panel F depicts a scenario where the strong Allee threshold ($\alpha_s = 150$) surpasses the initial resistant population. Consequently, the resistant cells undergo negative growth and are unable to maintain their viability. In contrast, the untreated baseline ($\beta = 0$) exhibits a gradual decrease towards a lower plateau, whereas the application of oncolytic virus therapy significantly hastens this decline, ultimately leading to the complete extinction of the resistant population [13, 17, 33].

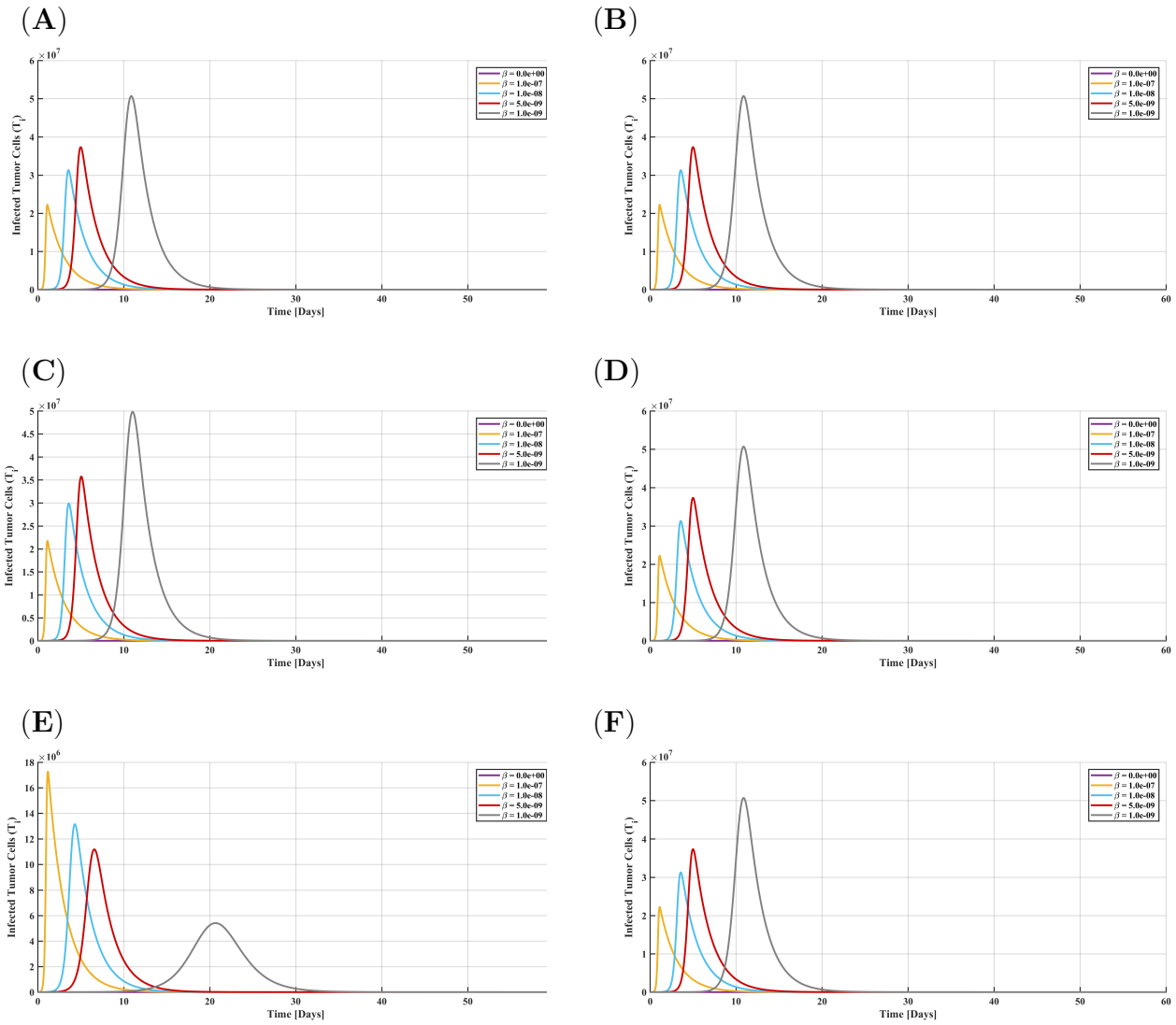

FIG. 3.6. **Allee effect on infected tumor cell population during OVT.**

(A),(C), and (E) represent the plots of the infected tumor cell population dynamics in the presence of weak Allee effect thresholds of $\alpha_w = 20,\ 2 \times 10^6, \text{and}\ 2 \times 10^9$ respectively. Similarly, (B),(D), and (F) illustrate the plots of the infected tumor cell population dynamics in the presence of strong Allee effect thresholds of $\alpha_s = 50,\ 100, \text{and}\ 150$ respectively. All plots display the system trajectories obtained by varying the infection rate β, ($\beta = 0,\ 1.0 \times 10^{-9},\ 5.0 \times 10^{-9},\ 1.0 \times 10^{-8},\ 1.0 \times 10^{-7}$ pfu^{-1} day^{-1}), in addition to varying Allee effect parameters while other parameters in **Tab.** 3.2 are kept at their baseline values.

Figure 3.6 presents the transient dynamics of the infected tumor cell population (T_i) during oncolytic virotherapy. As predicted, the control scenario without treatment ($\beta = 0$) results in a flat trajectory with no infected cells. After the introduction of the virus, the infected population shows a characteristic spike, increasing as the virus effectively invades susceptible cells, before quickly declining as viral lysis destroys the host cells [4, 41, 63].

Across all panels, a higher viral infection rate β consistently speeds up this process, causing the peak of infected cells to occur earlier due to the rapid conversion and subsequent destruction of the uninfected population [4, 41]. For moderate weak Allee thresholds (panels A and C) and all tested strong Allee thresholds (panels B, D, and F), the macroscopic trajectories of the infected cells remain nearly the same. The strong Allee thresholds ($\alpha_s = 50, 100, 150$) are relatively small compared to the total tumor volume, failing to significantly alter the peak infection dynamics, instead ensuring complete tumor clearance once the population is reduced to microscopic levels.

In contrast, panel E shows that a large weak Allee threshold ($\alpha_w = 2.0 \times 10^9$) significantly dampens the infection trajectory. This high threshold severely restricts the initial growth of the susceptible tumor cells, resulting in a much smaller pool of available hosts for the virus [4, 41, 63]. Consequently, the absolute peak number of infected cells is diminished by an entire order of magnitude compared to the other scenarios, and the progression of the infection is notably delayed at the lowest effective viral dose.

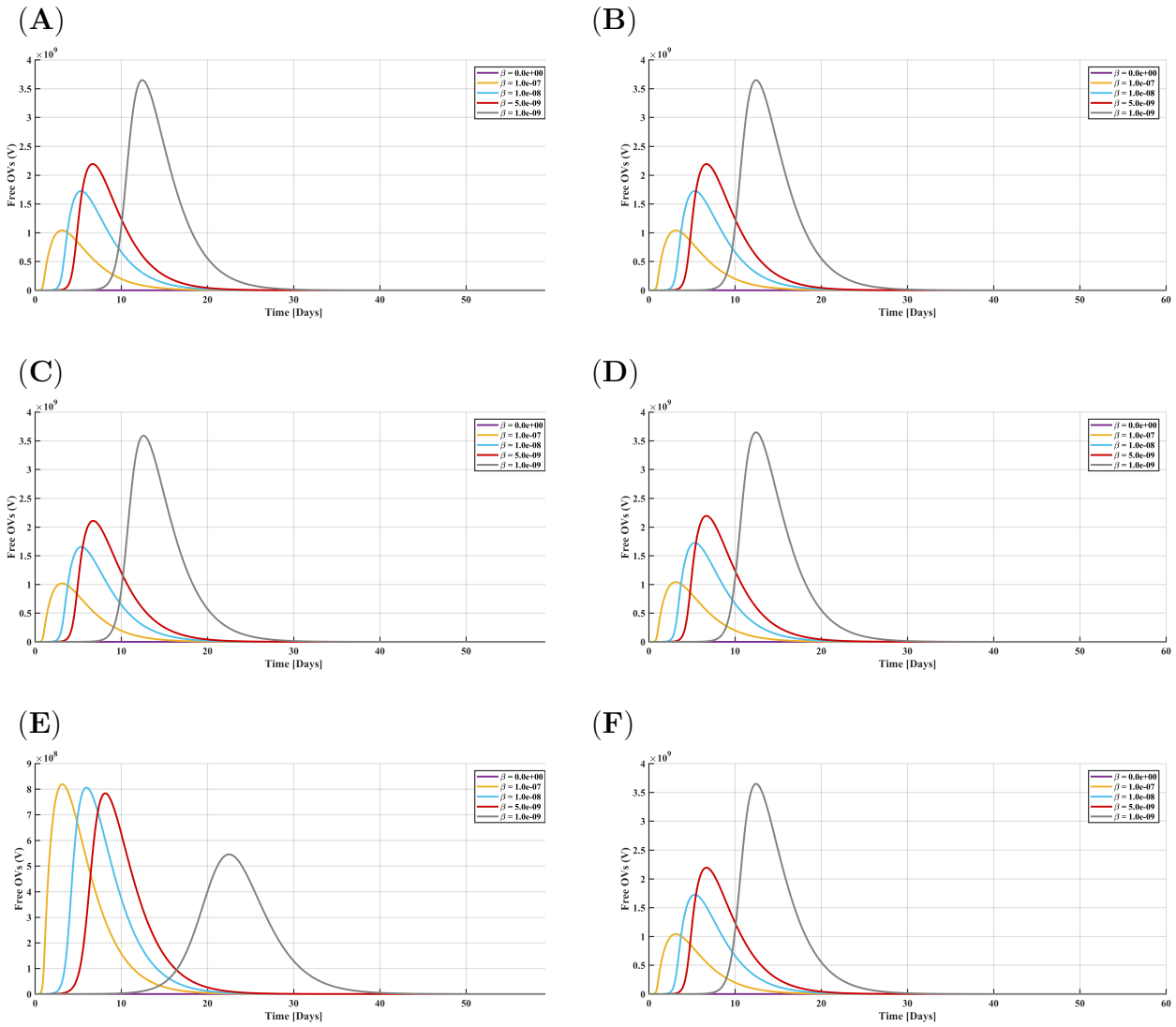

FIG. 3.7. **Allee effect on Free Oncolytic Viruses during OVT.**

(A),(C), and (E) represent the plots of the free oncolytic viruses cell population dynamics in the presence of weak Allee effect thresholds of $\alpha_w = 20,\ 2 \times 10^6, \text{and}\ 2 \times 10^9$ respectively. Similarly, (B),(D), and (F) illustrate the plots of the free oncolytic viruses cell population dynamics in the presence of strong Allee effect thresholds of $\alpha_s = 50,\ 100, \text{and}\ 150$ respectively. All plots display the system trajectories obtained by varying the infection rate β,
($\beta = 0,\ 1.0 \times 10^{-9},\ 5.0 \times 10^{-9},\ 1.0 \times 10^{-8},\ 1.0 \times 10^{-7}$ pfu^{-1} day^{-1}), in addition to varying Allee effect parameters while other parameters in **Tab.** 3.2 are kept at their baseline values.

Figure 3.7 depicts the dynamics of the free oncolytic virus population (V) as influenced by varying Allee effect thresholds. Consistent with the dynamics of infected cells noted earlier, scenarios with moderate weak Allee thresholds (panels A and C) and all strong Allee thresholds tested (panels B, D, and F) show nearly identical macroscopic trajectories. In these scenarios, the free virus population quickly surges as infected cells lyse and release new virions, followed by a gradual decline once the susceptible tumor cells are depleted [4]. A strikingly counterintuitive dynamic in these panels is that lower infection rates, such as $\beta = 1.0 \times 10^{-9}$ pfu^{-1} day^{-1}, lead to a delayed but significantly higher peak of free viruses compared to the highest infection rates. This occurs because a slower initial viral propagation allows the uninfected tumor population to grow further before being overtaken, ultimately resulting in a much larger reservoir of host cells that subsequently burst to produce a massive wave of free viruses.

On the other hand, panel E illustrates the systemic consequences of an extremely high weak Allee threshold ($\alpha_w = 2 \times 10^9$). This substantial threshold severely restricts the baseline proliferation of the tumor, thereby physically depriving the virus of its necessary replication factories. As a result, the overall peak concentration of free viruses is suppressed by an entire order of magnitude compared to the other simulated scenarios. Additionally, the pronounced, delayed viral spike observed at lower infection rates in the other panels is significantly flattened here. This indicates that when tumor growth is strictly limited by a high weak Allee proliferation penalty, the total burst yield of the virotherapy is proportionally constrained due to the lack of available host cells [4, 41, 63].

Chapter 4

Conclusions

In conclusion, the mathematical modeling of oncolytic virus therapy (OVT) shows that high rates of viral infection can effectively eliminate susceptible tumor cells [4, 41, 62, 63]. However, this success often leads to the competitive release and eventual dominance of therapy-resistant cancer cells [10, 41, 64, 65]. Without an Allee effect, tumors can grow from very low densities, making complete eradication nearly impossible. This constant presence of a cancer recurrence risk remains, no matter how effective the viral treatment is [13, 15, 16, 33].

Adding the Allee effect to tumor dynamics changes these therapeutic outcomes and provides an important way to fully eliminate tumors. A strong Allee effect creates a critical survival threshold. While this threshold might seem small compared to the overall tumor size and not dramatically change the peak of the initial viral infection, it plays an important biological role. When virotherapy reduces both susceptible and resistant tumor groups below this threshold, the strong Allee effect guarantees their eventual extinction and completely prevents tumor recurrence [13, 15, 33, 68].

Additionally, a weak Allee effect acts as an important regulatory force within the tumor microenvironment. A significant weak Allee penalty limits the baseline growth potential of the tumor. This is crucial because it reduces the most dangerous clinical outcome of virotherapy-competitive release. Even when the virus wipes out uninfected competitors, a high weak Allee threshold prevents resistant strains from reproducing effectively, keeping

the resistant population stagnant [13, 15].

The model reveals a surprising aspect of viral replication: lower infection rates can lead to larger subsequent releases of free virions [4]. Allowing a slight growth of the initial tumor population means a lower infection rate creates a bigger reservoir of host "factories" before the virus decreases the population. This study shows that improving the effectiveness of oncolytic virotherapy is not just about increasing viral infectivity. Long-term success requires a collaborative approach that uses viral lysis to push different, competing tumor subpopulations below their specific Allee thresholds. This strategy exploits the tumor's inherent ecological weaknesses to ensure full and lasting eradication [13, 15].

4.0.1 Limitations and future work

This study offers valuable insights into the relationship between oncolytic virotherapy (OVT), tumor resistance, and Allee effects. However, it also has limitations that point to areas for future research. First, the model assumes that cells and viruses in the tumor microenvironment are evenly mixed, using ordinary differential equations. In reality, solid tumors show spatial differences [69]. Physical barriers, blood vessel distribution, and limits on diffusion affect how well the virus penetrates and how resistant clones are arranged [70–72]. Using partial differential equations to address these spatial dynamics would improve the model's ability to predict clinical outcomes. Second, our model treats Allee thresholds as fixed. In biological terms, these thresholds can change over time due to evolving cell types or varying resource availability [15, 17]. Future studies should look into time-dependent or random Allee thresholds for a better understanding of biological variability. Finally, this model does not take the host immune response into account. The immune response can limit OVT through viral clearance, but it can also support it through bystander effects and anti-tumor immunity [31, 32]. Adding an immune component would create a more complete framework for studying combination therapies.

In conclusion, this research shows that incorporating the Allee effect into the mathematical modeling of OVT greatly improves our understanding of tumor elimination and resistance management. While high rates of viral infection can destroy susceptible cells, they also risk generating competitive release, which can lead to therapy-resistant clones [10, 41, 64, 65].

Our results suggest that the Allee effect takes advantage of weaknesses in the tumor's ecology to address this problem. A strong Allee effect establishes a clear survival threshold that guarantees both mathematical and biological extinction once OVT reduces tumor populations to microscopic sizes, fully preventing a recurrence of the disease [13, 15, 33, 68]. Meanwhile, a higher weak Allee effect threshold imposes a significant growth penalty that keeps newly resistant strains in a stagnant state, even when space and resources are available [13, 15]. Ultimately, these findings imply that effective OVT strategies should not only focus on increasing viral infectivity; they must also be designed to strategically influence system dynamics so that interacting tumor subpopulations fall below their critical Allee thresholds for lasting and multi-clonal tumor eradication.

Bibliography

[1] Bray F, Laversanne M, Sung H, Ferlay J, Siegel RL, Soerjomataram I, et al. Global cancer statistics 2022: GLOBOCAN estimates of incidence and mortality worldwide for 36 cancers in 185 countries. CA: a cancer journal for clinicians.2024;74(3):229-63.

[2] Fiandaca G. Tumour phenotypic heterogeneity in a niche-construction evolutionary perspective: investigating the impact of trade-offs via a mathematical approach.2022

[3] Nouni A, Hattaf K, Yousfi N. Dynamics of a mathematical model for cancer therapy with oncolytic viruses. Commun Math Biol Neurosci.2019;2019:Article-ID.

[4] Otero JG, Alcamí AÁA, Belmonte-Beitia J. Dynamics and analysis of a mathematical model of neuroblastoma treated with Celyvir. Applied Mathematical Modelling.2022;110:131-48.

[5] Carson EL. Mathematical Modelling of T Cell Infection during Oncolytic Viral Therapy. CA: a cancer journal for clinicians.2020

[6] Lawler SE, Speranza MC, Cho CF, Chiocca EA. Oncolytic viruses in cancer treatment: a review. JAMA oncology.2017;3(6):841-9.

[7] Wodarz D. Viruses as antitumor weapons: defining conditions for tumor remission. Cancer research.2001;61(8):3501-7.

[8] Bell JC. How oncolytic virus therapy is changing cancer treatment. Cancer Res Inst.2020;19:2022.

[9] Baabdulla AA, Hillen T. Oscillations in a spatial oncolytic virus model. Bulletin of Mathematical Biology.2024;86(8):93.

[10] Jankul F. Tumor heterogeneity in the clinic: is it a real problem? Therapeutic advances in medical oncology.2014;6(2):43-51.

[11] McDonald TO, Cheng YC, Graser C, Nicol PB, Temko D, Michor F. Computational approaches to modelling and optimizing cancer treatment. Nature Reviews Bioengineering.2023;1(10):695-711.

[12] Zhang J, Cunningham J, Brown J, Gatenby R. Evolution-based mathematical models significantly prolong response to abiraterone in metastatic castrate-resistant prostate cancer and identify strategies to further improve outcomes. Elife.2022;11:e76284.

[13] Hernández-López E, Wang J. A mathematical perspective on the influence of Allee effects in oncolytic virotherapy. Mathematics. 2025;13(5):744.

[14] Benzekry S, Lamont C, Beheshti A, Tracz A, Ebos JML, Hlatky L, et al. Classical mathematical models for description and prediction of experimental tumor growth. PLoS computational biology.2014;10(8):e1003800.

[15] Delitala M, Ferraro M. Is the Allee effect relevant in cancer evolution and therapy? AIMS mathematics.2020;5(6):7649-60.

[16] Johnson KE, Howard G, Mo W, Strasser MK, Lima EABF, Huang S, et al. Cancer cell population growth kinetics at low densities deviate from the exponential growth model and suggest an Allee effect. PLoS biology. 2019;17(8):e3000399.

[17] Böttger K, Hatzikirou H, Voss-Böhme A, Cavalcanti-Adam EA, Herrero MA, Deutsch A. An emerging Allee effect is critical for tumor initiation and persistence. PLoS computational biology. 2015;11(9):e1004366.

[18] Bastian F, Alkhayuon H, Mulchrone K, O'riordain M, Wieczorek SM. Cancer model with moving extinction threshold reproduces real cancer data. Journal of the Royal Society Interface.2025;22(231).

[19] Novozhilov AS, Berezovskaya FS, Koonin EV, Karev GP. Mathematical modeling of tumor therapy with oncolytic viruses: effects of parametric heterogeneity on cell dynamics. Biology direct.2006;1(1):30.

[20] Abernathy Z, Abernathy K, Stevens J. A mathematical model for tumor growth and treatment using virotherapy. AIMS Mathematics.2020;5(5):4136.

[21] Jenner AL, Coster ACF, Kim PS. Treating cancerous cells with viruses: insights from aminimal model for oncolytic virotherapy. Letters in Biomathematics.2018;5(2):117-36.

[22] Xu J, Xia Z, Wang S, Xia Q. Resistance to oncolytic virotherapy: Multidimensional mechanisms and therapeutic breakthroughs. International Journal of Molecular Medicine.2025;56(5):171.

[23] El-Sayes N, Vito A, Mossman K. Tumor heterogeneity: a great barrier in the age of cancer immunotherapy. Cancers.2021;13(4):806.

[24] Bhatt DK, Chammas R, Daemen T. Resistance mechanisms influencing oncolytic virotherapy, a systematic analysis. Vaccines.2021;9(10):1166.

[25] Allee WC. Animal aggregations. The Quarterly Review of Biology.1927;2(3):367-98.

[26] dos Santos RV, Ribeiro FL, Martinez AS. Models for Allee effect based on physical principles Journal of theoretical biology.2015;385:143-52.

[27] Dong Y, Liu H, Ye J, Ma G, Wei Y. The effects of the weak allee effect and disease on the dynamics of a predator–prey system: Stability and bifurcation properties. Axioms. 2025;14(7):531.

[28] Fadai NT, Simpson MJ. Population dynamics with threshold effects give rise to a diverse family of Allee effects. Bulletin of mathematical biology. 202O;82(6):74.

[29] Wittmann MJ, Gabriel W, Metzler D. Genetic diversity in introduced populations with an Allee effect. Genetics. 2014;198(1):299-310.

[30] Fadai NT, Johnston ST, Simpson MJ. Unpacking the Allee effect: determining individual-level mechanisms that drive global population dynamics. Proceedings of the Royal Society A: Mathematical, Physical and Engineering Sciences. 2020;476(2241):e1004366.

[31] Mohammadnejad N, Hillen T. Qualitative optimization of oncolytic virotherapy and immune therapy combination treatments. bioRxiv.2025;2025-09.

[32] G Marelli NLYW A Howells. Oncolytic viral therapy and the immune system: a double-edged sword against cancer. Frontiers in immunology.2018;9:866.

[33] Gerlee P, Altrock PM, Malik A, Krona C, Nelander S. Autocrine signaling can explain the emergence of Allee effects in cancer cell populations. PLoS computational biology. 2022;18(3):e1009844.

[34] Guo Y, Niu B, Tian JP. Backward Hopf bifurcation in a mathematical model for oncolytic virotherapy with the infection delay and innate immune effects. Journal of biological dynamics. 2019;13(1):733-48.

[35] Eftimie R, Macnamara CK, Dushoff J, Bramson JL, Earn DJD. Bifurcations and chaotic dynamics in a tumour-immune-virus system. Mathematical Modelling of Natural Phenomena. 2016;11(5):65-85.

[36] Hernández-López E, Wang X, Wang J. Mathematical modeling of allee effects in tumor dynamics: Insights into chemotherapy and immunotherapy optimization. Discrete and Continuous Dynamical Systems-B. 2026;31:219-54.

[37] Mahasa KJ, Eladdadi A, Pillisa LD, Ouifki R. Oncolytic potency and reduced virus tumor-specificity in oncolytic virotherapy. A mathematical modelling approach. PLoS One. 2017;12(9):e0184347.

[38] Gatenby RA, Vincent TL. An evolutionary model of carcinogenesis. Cancer research.2003;63(19):6212-20.

[39] Ambegoda P, Wei HC, Jang SRJ. The role of immune cells in resistance to oncolytic viral therapy. Mathematical Biosciences and Engineering.2024;21(5):5900-46.

[40] Ambegoda-Liyanage P, Jang SRJ. Resistance in oncolytic viral therapy for solid tumors. Applied Mathematics and Computation.2024;469:128546.

[41] Karev GP, Novozhilov AS, Koonin EV. Mathematical modeling of tumor therapy with oncolytic viruses: effects of parametric heterogeneity on cell dynamics. Biology direct.2006;1(1):30.

[42] Wodarz D, Komarova N. Towards predictive computational models of oncolytic virus therapy: basis for experimental validation and model selection. PloS one.2009;4(1):e4271.

[43] Wang G, Yi M, Tang S. Dynamics of an antitumour model with pulsed radioimmunotherapy. Computational and Mathematical Methods in Medicine.2022;2022(1):4692772.

[44] Vercken E, Groussier G, Lamy L, Mailleret L. The hidden side of the Allee effect: correlated demographic traits and extinction risk in experimental populations. Peer Community Journal.2021;1.

[45] Surendran A, Plank MJ, Simpson MJ. Population dynamics with spatial structure and an Allee effect. Proceedings of the Royal Society A: Mathematical, Physical and Engineering Sciences.2020;476(2242).

[46] Storey KM, Lawler SE, Jackson TL. Modeling Oncolytic Viral Therapy, Immune Checkpoint Inhibition, and the Complex Dynamics of Innate and Adaptive Immunity in Glioblastoma Treatment. Frontiers in Physiology. 2020;11:151.

[47] Yu JL, Jang SRJ, Liu KY. Exploring the interactions of oncolytic viral therapy and immunotherapy of anti-CTLA-4 for malignant melanoma mice model. Cells.2023;12(3):507.

[48] Bhatt DK, Janzen T, Daemen T, Weissing FJ. Modelling the spatial dynamics of oncolytic virotherapy in the presence of virus-resistant tumour cells PLoS computational biology.2022;18(12):e1010076.

[49] Almuallem N, Trucu D, Eftimie R. Oncolytic viral therapies and the delicate balance between virus-macrophage-tumour interactions: A mathematical approach. Mathematical Biosciences and Engineering.2021;18(1):764-99.

[50] Ghorbal K, Sogokon A. Characterizing positively invariant sets: Inductive and topological methods. Journal of Symbolic Computation.2022;113:1-28.

[51] Lakshmikantham V, Bainov DD, Simeonov P. Theory of impulsive differential equations. World scientific.1989;6.

[52] Oguntuase JA. On Gronwall Inequality. Analele Stiitifice Ale Universtat "ALLCUZA" IASI, Tomul XLVII, S. Ia Matimatica, f. I51-56.2001

[53] Diekmann O, Heesterbeek JAP, Metz JAJ. On the definition and the computation of the basic reproduction ratio R 0 in models for infectious diseases in heterogeneous populations. Journal of mathematical biology.1990;28(4):365-82.

[54] Reckell T, Sterner B, Jevtić P. The basic reproduction number for petri net models: A next-generation matrix approach Applied Sciences.2025;15(23):12827.

[55] Sanchez DA. Ordinary differential equations and stability theory: an introduction.1979

[56] Moghadamnia Y, Moslemi D. A stochastic mathematical model of avascular tumor growth patterns and its treatment by means of noises. Caspian journal of internal medicine.2017;8(4):258.

[57] Bodson M. Explaining the Routh–Hurwitz criterion: A tutorial presentation [focus on education]. IEEE Control Systems Magazine.2020;40(1):45-51.

[58] Izhikevich EM. Equilibrium. Scholarpedia.2007;2(10):2014.

[59] Hoti M. Analysis of Non-Hyperbolic Equilibrium Point for Ordinary Planar Systems.2021

[60] Barratt H, Kirwan M, Shantikumar S. Epidemic theory (effective & basic reproduction numbers, epidemic thresholds) & techniques for analysis of infectious disease data (construction & use of epidemic curves, generation numbers, exceptional reporting & identification of significant clusters). Health Knowledge.2018

[61] Aronson JK, Brassey J, Mahtani KR. "When will it be over?": An introduction to viral reproduction numbers, R 0 and R e. Av ailablefrom: https://www cebm net/covid-19/when-willit-be-over-an-introduction-toviralreproduction-numbers-r0-and-re/(Accessed 13th July 2022).2020

[62] Jang SRJ, Wei HC. On a mathematical model of tumor-immune system interactions with an oncolytic virus therapy. Discrete & Continuous Dynamical Systems-B. 2021;2021.

[63] Omer S, Mambili-Mamboundou H. Assessing the impact of immunotherapy on oncolytic virotherapy in the treatment of cancer. Journal of Applied Mathematics and Computing.2024;70(5):4793-825.

[64] Wodarz D. Use of oncolytic viruses for the eradication of drug-resistant cancer cells. Journal of The Royal Society Interface.2008;6(31):179.

[65] West J, Ma Y, Newton PK. Capitalizing on competition: An evolutionary model of competitive release in metastatic castration resistant prostate cancer treatment. Journal of Theoretical Biology.2018;455:249-60.

[66] Hernández-López E, Núñez-López M, Hernández-Martínez LI, Wang J. Bifurcation Analysis of Tumor-Immune Dynamics and the Role of Strong and Weak Allee Effects in Cancer Immunoediting Process. International Journal of Bifurcation and Chaos.2018;36(02):2650020.

[67] Xiao D, Zhang H, Liu Y, Li Y, Li G, Ning Y. Oncolytic viruses: advanced strategies in cancer therapy. Signal Transduction and Targeted Therapy.2026;11(1):45.

[68] Bolnick DI, Ingram T, Stutz WE, Snowberg LK, Lau OL, Paull JS. Ecological release from interspecific competition leads to decoupled changes in population and individual niche width. Proceedings of the Royal Society B: Biological Sciences.2010;277(1689):1789.

[69] Sewalt L, Harley K, v Heijster P, Balasuriya S. Influences of Allee effects in the spreading of malignant tumours. Journal of theoretical biology.2016;394(1689):77-92.

[70] Kühnert D, Wu CH, Drummond AJ. Phylogenetic and epidemic modeling of rapidly evolving infectious diseases. Infection, genetics and evolution.2011;11(8):1825-41.

[71] Bhatt DK, Janzen T, Daemen T, Weissing FJ. Modelling the spatial dynamics of oncolytic virotherapy in the presence of virus-resistant tumour cells. PLoS computational biology.2022;18(12):e1010076.

[72] Pooladvand P. Mathematical models in oncolytic virotherapy and immunology. PLoS computational biology.2021